REPORT 1110

SOME FEATURES OF ARTIFICIALLY THICKENED FULLY DEVELOPED TURBULENT BOUNDARY LAYERS WITH ZERO PRESSURE GRADIENT [1]

By P. S. Klebanoff and Z. W. Diehl

SUMMARY

An account is given herein of an investigation conducted to determine the feasibility of artificially thickening a turbulent boundary layer on a flat plate. A description is given of several methods used to thicken artificially the boundary layer. It is shown that it is possible to do substantial thickening and obtain a fully developed turbulent boundary layer, which is free from any distortions introduced by the thickening process, and, as such, is a suitable medium for fundamental research. Measurements of mean velocity, spectrum of u-fluctuation, and intensity of u-fluctuation which served as criteria for determining the state of the layer are presented. Some features of the fully developed turbulent boundary layer with zero pressure gradient are discussed. The mean flow in the boundary layer is compared with the logarithmic laws of mean-velocity distribution derived for pipes and channels, and the existing theories dealing with the shape of the spectrum in isotropic turbulence are applied to the spectrum measured in the outer portion of the boundary layer. It is also shown that the turbulence in the outer portion of the boundary layer has an intermittent character similar to that found for wakes and jets.

INTRODUCTION

The lack of a satisfactory theory for turbulent shear flow and the development of the hot-wire anemometer as a powerful tool for turbulence research have directed attention to the quantitative measurement of the characteristics of turbulence in shear flow as a means of obtaining information on which to base a sound theory. The recent concept of local isotropy proposed by Kolmogoroff (references 1 and 2), that is, that, whatever the nature of the large-scale motions, the small-scale turbulence tends to be isotropic, has intensified the experimental program with the hope that the existing theories of isotropic turbulence may be useful. While a considerable amount of work has been done in various flow fields (references 3, 4, 5, and 6), attention is here centered on the boundary layer, not only because of its practical importance but to provide information which can be compared with that obtained in other types of shear flow and thus show differences and likenesses and in particular show whether certain phenomena are universal. It is felt that the results of the measurements can best be compared with the theory of isotropic turbulence if such complicating factors as pressure gradient, curvature, surface roughness, and compressibility are eliminated. Furthermore, the turbulence should be fully developed and the Reynolds number should be sufficiently high to bring the domain of local isotropy within the range of measurement. In addition the boundary layer should be as thick as possible in order to facilitate the use of multiwire hot-wire probes and minimize errors due to wire length.

These requirements mean that the surface should be smooth and flat and that high Reynolds number should be obtained by thickness rather than by high speed. Such requirements are difficult to meet, except in wind tunnels especially constructed for the purpose. The use of one wall of a conventional wind tunnel does not appear to be a satisfactory solution because of the likelihood of extraneous effects. The problem of obtaining a thick boundary layer was encountered at the National Bureau of Standards when a turbulent-boundary-layer investigation using a flat plate was undertaken. The test section of the tunnel was 19 feet long, but it was not feasible to use a plate longer than 12 feet. It was felt that the need for a thicker boundary layer than one which would normally develop on 12 feet of surface was sufficiently urgent here, and possibly in other laboratories with even less length available, to warrant an investigation of the possibilities of artificially thickening the layer. This involved not only methods of thickening but also setting up criteria by which to establish the identity of a fully developed layer over a smooth surface.

In determining the feasibility and validity of artificial thickening a number of measurements had to be made, including mean velocities, intensity of u-fluctuations, and the spectrum of u-fluctuations. As a consequence it is possible to show how such quantities are affected by thickening devices and what values they assume when the layer is no longer influenced by its beginnings. It is obviously very necessary to know whether there exists a "flat-plate boundary layer" of universal character depending only on Reynolds number. This is shown to be the case insofar as the observed quantities provide a proper sampling.

The investigation was conducted under the sponsorship and with the financial assistance of the National Advisory Committee for Aeronautics.

The authors wish to express their appreciation for the constant advice and active interest of Dr. G. B. Schubauer both in the experimental program and in the preparation of the report. Acknowledgment is made to Messrs. G. H. Adams and L. M. Kelly for their assistance in the experimental program. The authors also wish to thank Dr. C. M. Tchen and Dr. J. Laufer for their interest and stimulating discussions.

[1] Supersedes NACA TN 2475, "Some Features of Artificially Thickened Fully Developed Turbulent Boundary Layers with Zero Pressure Gradient" by P. S. Klebanoff and Z. W. Diehl, 1951.

SYMBOLS

x	distance along surface from leading edge of flat plate
y	distance normal to surface, measured from surface of flat plate
U	mean velocity in boundary layer
U_1	mean velocity in free stream, just outside boundary layer
u, v, w	x, y, and z components of instantaneous turbulent-velocity fluctuations
$\overline{u^2}, \overline{v^2}, \overline{w^2}$	mean-square values of u, v, and w
u'	root-mean-square value of u
ρ	density of air
ν	kinematic viscosity of air
P	static pressure
P_o	static pressure at $x=10.5$ feet
q_1	free-stream dynamic pressure
q_o	free-stream dynamic pressure at $x=10.5$ feet
q_s	dynamic pressure in boundary layer as measured with a surface tube
τ_o	shearing stress at surface
χ	absolute constant
A_o	constant
$A_1=(8\epsilon/9\chi)^{2/3}$	
$A_2=(\chi\epsilon/2\nu^2)^2$	
$U_\tau=\sqrt{\frac{\tau_o}{\rho}}$	
δ	boundary-layer thickness
δ^*	boundary-layer displacement thickness $\left(\int_0^\infty\left(1-\frac{U}{U_1}\right)dy\right)$
θ	boundary-layer momentum thickness $\left(\int_0^\infty\frac{U}{U_1}\left(1-\frac{U}{U_1}\right)dy\right)$
R_δ	Reynolds number based on boundary-layer thickness $\left(\frac{U_1\delta}{\nu}\right)$
R_θ	Reynolds number based on boundary-layer momentum thickness $\left(\frac{U_1\theta}{\nu}\right)$
R_x	longitudinal space correlation coefficient of u-fluctuation
L_x	longitudinal scale of u-fluctuation
λ	microscale in isotropic turbulence
ϵ	total dissipation of turbulent energy per unit mass per second
t	time
n	frequency, cycles per second
k_s	wave number in intermediate range where initial forces and viscosity both play role
k_x	one-dimensional wave number $\left(\frac{2\pi n}{U}\right)$
$k_{sx}=0.645k_s$	
k	three-dimensional wave number
$F(n)$	normalized one-dimensional spectral function associated with frequency n
$z=nL_x/U$	
z_s	constant
$F(z)=UF(n)/L_x$	
$E_x(k_x)$	one-dimensional spectral function associated with k_x
$E(k)$	three-dimensional spectral function associated with k

APPARATUS AND PROCEDURE

GENERAL ARRANGEMENT

The investigation was conducted in the 4½-foot wind tunnel at the National Bureau of Standards, using a flat plate 12 feet long mounted vertically along the center line of the test section, the leading edge being 6 feet from the upstream end of the test section. The plate was ¼-inch aluminum with a smooth surface and a sharp leading edge formed by a smooth symmetrical taper beginning 4 inches from the leading edge. The plate was fastened along the horizontal edges to one side of 3-inch channel irons anchored to the upper and lower tunnel walls, and so divided the test section into nearly equal passages. It was considered desirable to conduct the investigation in a tunnel of low turbulence so that the turbulence of the free stream would be negligible compared with that in the boundary layers. The turbulence level of the tunnel was 0.02 percent at 30 feet per second and 0.04 percent at 100 feet per second. An elevation view of the tunnel is shown in figure 1. More details as to the arrangement of damping screens used in obtaining the low turbulence are given in reference 7.

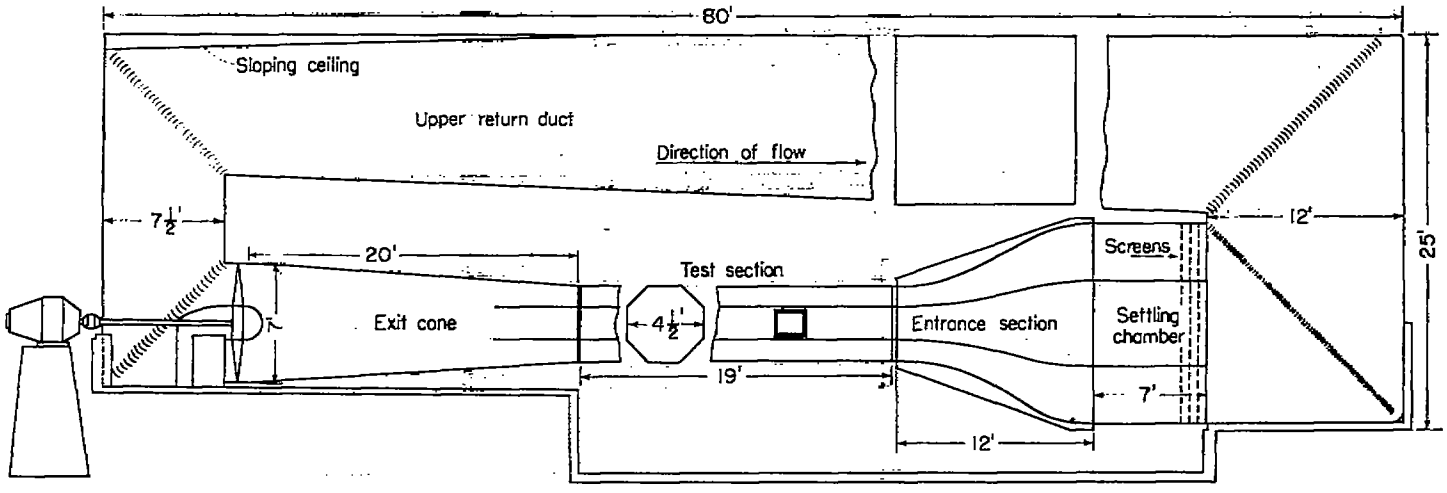

FIGURE 1.—Elevation view of NBS 4½-foot wind tunnel.

In order to obtain a condition of zero pressure gradient, a flexible second wall of sheet aluminum was mounted on the tunnel wall facing the working side of the plate. It was attached to the ends of screws threaded into the tunnel wall and thus provided an adjustable section to make the passage between the plate and the wall sufficiently diverging to offset the pressure drop resulting from boundary-layer growth.

Another important consideration was proper angle of attack to afford smooth flow entry at the leading edge on the working side of the plate. This was accomplished by displacing the upstream edge of the plate and by partial blocking of the passage on the working side. Since the obstructions causing the blocking had to be placed farther downstream than any usable portion of the plate, the passage was extended 4 feet by joining the trailing edge of the plate with a section of plywood.

Under these conditions the pressure distribution along the plate was found to be as shown in figure 2(a). From 2 feet on downstream the pressure is seen to be uniform on the average with variations of about 1 percent of q_o about the mean. These variations could not be removed by the adjustable wall because they were associated with a slight waviness of the surface of the plate.

Figure 2(b) shows the transition region at a speed of 108 feet per second for smooth entry conditions at the leading edge. The beginning of transition corresponds to a Reynolds number (based on length of laminar flow) of 3,175,000, and here transition results from the growth of more or less regular laminar-boundary-layer oscillations.

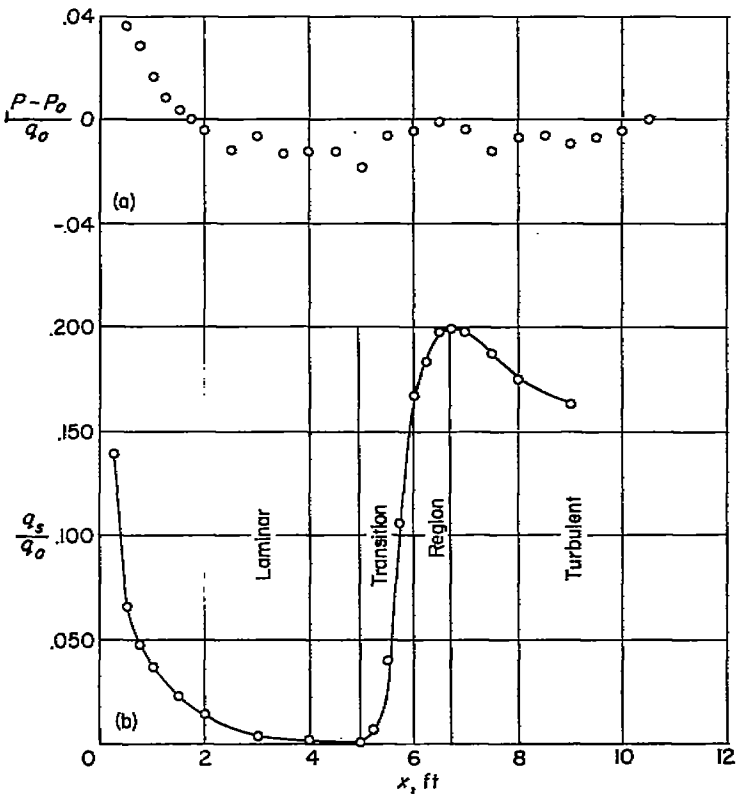

(a) Pressure distribution along flat plate.
(b) Variation of dynamic pressure as measured with a surface tube through transition region. U_1=108 feet per second.

FIGURE 2.—Pressure-distribution and transition data.

INSTRUMENTATION AND TECHNIQUES

Traversing mechanism.—In order to traverse in a horizontal plane normal to the surface the unit shown in figure 3 was used. A micrometer screw with 0.5-millimeter pitch is driven through a set of beveled gears and a shaft by a selsyn motor remotely controlled. To provide for ease of alinement, the pressure probes and hot-wire holders are attached so that they can move fore and aft and rotate in a vertical plane. By means of the bracket shown in the figure the unit is bolted to a streamlined strut so that the end opposite the gears is forced against the surface. Channel irons anchored to the floor and ceiling of the tunnel served as guide rails for the strut, and traversing longitudinally was done by moving the strut fore and aft by means of a chain and sprocket manually operated from outside the tunnel.

Measurement of pressure distribution, transition, and mean velocity.—Measurements of pressure distribution and transition were made with the pitot-static head shown in figure 4. The impact tube makes contact with the surface, and the static tube is opposite the point of contact ¼ inch away from the surface. The static and impact tubes are made of 0.04-inch nickel tubing with 0.003-inch wall thickness. The static tube is made according to the conventional design for such a tube, and the impact tube is flattened at the end to form a rectangular opening 0.014 inch wide. The static tube was used for the measurement of pressure distribution and both impact and static tubes for the measurement of transition. The head was attached by a long arm (containing the pressure leads) to the strut and could be moved back and forth in the x-direction while the forklike guides maintained proper relation to the surface. The determination of the transition point with the surface tube depends on the increase in impact pressure close to the surface when the layer becomes turbulent. The abruptness of the increase is shown in figure 2(b). The beginning and ending of the transition region coincide with the beginning and ending of the rise. This was checked with the hot-wire head shown in figure 4. This sledlike head was attached to the strut so that it could be moved fore and aft like the pitot-static head. The hot-wire was at a fixed distance of 0.03 inch from the surface, and visual observation of the fluctuations on an oscilloscope for different positions along the surface confirmed the indications of the surface tube. Measurements of mean velocity were made with a pitot-static combination similar

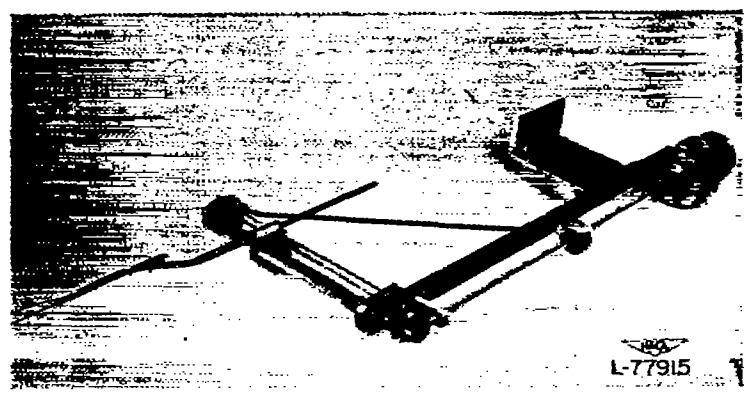

FIGURE 3.—Traversing mechanism with total-head and static tubes attached. Reference scale in inches.

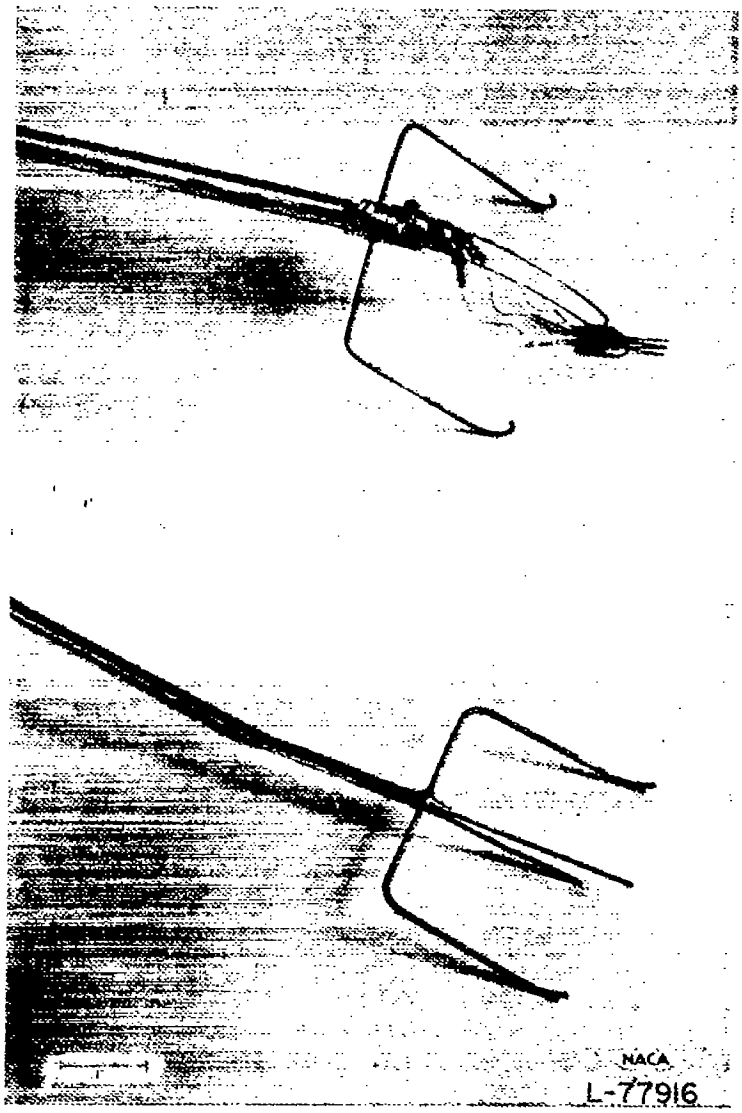

FIGURE 4.—Sliding hot-wire head and surface pitot-static tube.

to the one described above but without the guides. It is shown with the traversing unit in figure 3. No correction was made for the effect of turbulence on the readings.

Measurement of intensity and spectrum of u-fluctuation.—A description of the method and the hot-wire equipment used for measuring the intensity of u-fluctuation is given in detail in reference 8. Platinum wire 0.0001 inch in diameter and 0.5 millimeter long was used. This was wire drawn by the Wollaston process, and the method of making a hot-wire probe was to etch away the silver coating and then soft-solder the wire to the tips of fine sewing needles. The time constant of the wire was approximately 0.25 millisecond and was determined by the square-wave method described by Kovásznay (reference 9). Compensation for the time lag was made by a resistance-capacitance network in the amplifier. The response of the uncompensated amplifier was flat from 10 to 5000 cycles per second and fell off to about 50 percent at 10,000 cycles per second. The mean-square output was read on a microammeter working out of a thermocouple circuit.

In order to measure the spectrum of u-fluctuation the output circuit of the hot-wire amplifier was bypassed and the signal fed into an Electrical Research Products, Inc., sound analyzer with a frequency range from 10 to 10,000 cycles per second and a choice of fixed band widths of nominally 5 or 50 cycles per second. The rectifier type of output circuit of the analyzer was replaced by an additional stage of amplification and a thermocouple and meter. The purpose of this was to read mean-square currents and also to obtain a highly damped indicator. In reading the output, averages were taken over a period of 1 minute. The mean-square voltage corresponding to the compensated hot-wire signal passed by the band was obtained by first reading the hot-wire signal on the output meter and then matching this signal with a known sinusoidal signal fed into the system from a General Radio microvolter. The known signal had the frequency corresponding to the center of the band. The mean-square hot-wire voltage per unit frequency was then obtained by dividing by the effective band width. The effective band width was defined as the rectangular band width having the same area as the experimentally determined band shape. These were

Effective (cps)	Nominal (cps)
7.07	5
57.9	50

It was found to be advantageous to use the 7.07 band from 10 to 1000 cycles per second and the 57.9 band from 1000 to 10,000 cycles per second.

ARTIFICIAL THICKENING OF BOUNDARY LAYER

It is at once obvious that objects protruding outward from a surface create more drag than the surface that they cover and hence offer a means of producing a layer of de-energized flow in a comparatively short distance in the streamwise direction. The energy of the main flow is diverted into eddy motion in wakes, and, while the flow is turbulent, it does not have the same dynamic structure as a fully developed turbulent boundary layer over a smooth surface. The question is, after leaving drag-producing objects, what length of smooth surface is needed for the layer to become the same as a smooth-surface generated layer. It would seem that the length would be less than that required to generate a layer of the same thickness, but this is by no means a foregone conclusion.

Since the ultimate aim of the work was to produce a layer approximately 3 inches thick, this thickness having been chosen as sufficient for the convenient use of hot-wire probes, no effort was made to find the maximum thickness that could be produced in a given length. Emphasis was placed rather on simplicity of method and adequacy of tests.

The turbulent boundary layer along the plate was first obtained by the conventional method of free transition, that is, from the instability of laminar-boundary-layer oscillations. Then, various devices such as rods, screens, and distributed roughness were used on the laminar layer to force transition and de-energize the flow. Attention was given to maintaining the condition of zero pressure gradient for the modified layers by adjusting the "false" wall. The first attempt at

thickening the layer was to use rods, which were 0.04, 0.11, 0.18, and 0.25 inch in diameter. These were placed singly in the laminar layer and in contact with the surface at 4 feet from the leading edge. As will be seen, these were not satisfactory because of the length required for their distorting effect to disappear. The second method consisted in placing wire screens of various mesh sizes at different angles to the plate and close to the leading edge, so that the screen and plate formed a narrow wedge opening into the wind. A 24-mesh screen of 0.0075-inch wire diameter, which was 1 foot wide, making an angle of 0.5° with the plate and extending from floor to ceiling, was a satisfactory thickening device, but it was not considered practical because of the possibility of accidental shifting. The third and final method consisted in cementing sandpaper to the surface beginning at the leading edge and extending for distances up to 2 feet downstream. Various amounts of sand roughness were tried until the layer was of the desired thickness. The final arrangement of the roughness was No. 16 floor-sanding paper, cemented to the plate from the leading edge to 2 feet downstream and extending from floor to ceiling.

Initially the one-dimensional spectrum of u-fluctuations was thought to be the best over-all test to be applied to the resulting layers. Accordingly, for a basis of comparison, considerable attention was given to the spectrum of the fully developed layer resulting from free transition. It was found later that the mean-velocity profile was a still more sensitive test of the condition of the layer. Finally, the distribution of u' across the layer was added to the list of criteria. These three, compared in different parts of the layers and compared with other available data, served as the sample phenomena to determine the state of the layer.

RESULTS AND DISCUSSION

MEAN-VELOCITY MEASUREMENTS

With free transition beginning at the 5-foot position, as shown in figure 2, mean-velocity distributions were determined at $x=7.5$, 8.5, 9.5, and 10.5 feet at a free-stream speed of 108 feet per second. These are shown in figure 5. A lower value of U_1 would have shifted the transition point too close to the trailing edge of the plate. Figure 6 shows the same velocity profiles on a nondimensional basis. In order to avoid the arbitrariness of δ, the nondimensional distance from the wall y/δ^* is used. It is seen from figure 6 that downstream from the extreme position of the transition point, that is, $x=6.75$ feet, the profiles exhibit similarity. The two-dimensional nature of the flow was checked by making velocity measurements 10 inches below and above the center line at $x=10.5$ feet and comparing with the velocity distribution at the center line. Agreement among the three sets of distributions confirmed the two-dimensionality of the flow.

The velocity measurements for the 0.04- and 0.25-inch rods are shown in figures 7 and 8. At a free-stream speed $U_1=108$ feet per second, the flow, after passing over the rods, became turbulent in the separated layer and reattached to the surface in the turbulent state. At a lower free-stream speed $U_1=30$ feet per second for the 0.04-inch rod, visual observation of an oscilloscope trace obtained by traversing downstream from the rod at a distance of 0.03 inch from the surface, with a hot-wire anemometer, showed the reappearance of laminar-boundary-layer oscillations, indicating that the separated layer returned to the surface as a laminar layer without the occurrence of transition. This effect was also noticed by Liepmann and Fila (reference 10). Figures 9 and 10 give some of the representative profiles for the 0.04- and 0.25-inch rod in nondimensional form. The profile for $x=5.17$ feet in figure 9 differs from those at 6.0 and 10.5 feet by more than the experimental scatter. This would place the beginning of similarity for the 0.04-inch rod between $x=5.17$ feet and $x=6.0$ feet. In figure 10 there is no evidence of the beginning of similarity downstream of the 0.25-inch rod, and comparison of the profile at $x=10.5$ feet with other distributions, at the same Reynolds number, which do exhibit similarity indicated that, even at $x=10.5$ feet, 6.5 feet downstream from the rod, the velocity distribution is not yet similar. Figures 11 (a) and 11 (b) show the distributions for the 0.04-, 0.11-, 0.18-, and 0.25-inch rods at $x=6.0$ feet and $x=10.5$ feet, respectively. It is seen that the deviation among the profiles is less at $x=10.5$ feet than at $x=6.0$ feet, illustrating the trend toward similarity and the dependence of the similarity position on the rod diameter. The trend in figure 10 is in the opposite direction of a Reynolds number effect, but the Reynolds number change involved is small enough to be negligible compared with the differences indicated. It is expected that immediately downstream from the rod there would be an influence on dP/dx and dP/dy, but there is no evidence that it persisted to any great length downstream. If the similarity position for the 0.04-inch rod is taken at $x=5.5$ feet, that is, 1.5 feet downstream from the rod, the ratio of similarity distance to rod diameter is 450. Assuming a linear effect of the rod diameter on the similarity distance would put the similarity position for the 0.11-, 0.18-, and 0.25-inch rods at $x=8.2$, 10.9, and 13.5 feet, respectively. This is applied only for the condition of the rod at 4 feet and $U_1=108$ feet per second. The wind speed and the position of the rod in the layer, that is, the size of the rod compared with the boundary-layer thickness, may be other variables which have an effect. The conclusion from this is that too much length is required for distortions to disappear for rods to be practical thickening devices.

The velocity distributions at a free-stream speed $U_1=43$ feet per second for a 24-mesh screen making an angle of 0.5° with the plate are shown in figure 12. Although no summary plot is given, it may be stated that the profiles from $x=3.5$ feet to $x=10.5$ feet exhibited similarity. The boundary-layer thickness at $x=10.5$ feet is approximately 3 inches as compared with 1.4 inches for the condition of free transition. The effect of wider angle or greater solidity was to move the similarity position farther downstream and to give a thicker layer. For example, the profiles produced by a 24-mesh screen, at an angle of 2.5° with the plate, did not show similarity at $x=5.0$ feet. At $x=9.5$ feet the flow was similar, and the layer was 5.2 inches thick. Since no measurements were made between $x=5.0$ feet and $x=9.5$ feet, the position at which similarity first occurred is unknown.

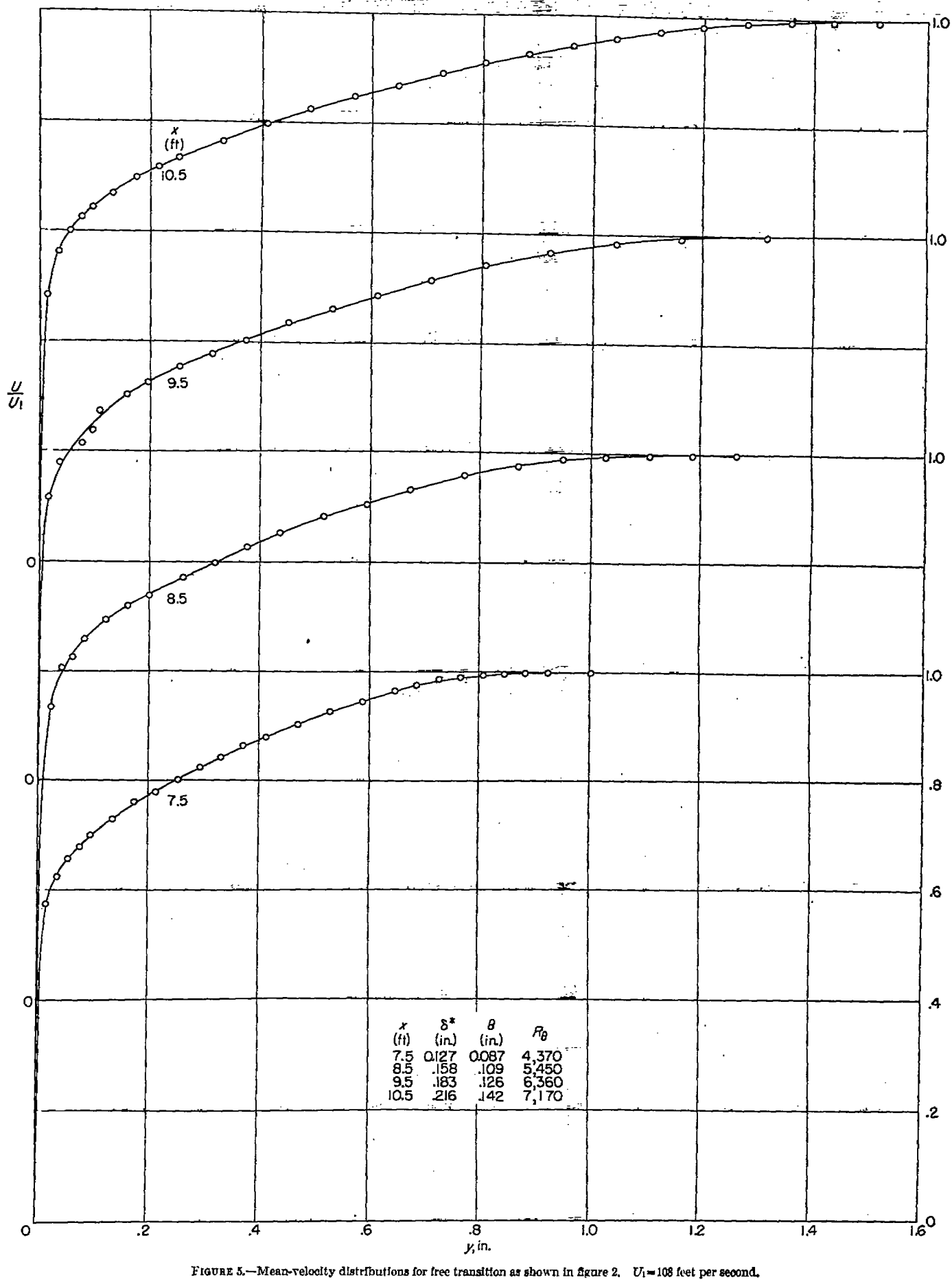

FIGURE 5.—Mean-velocity distributions for free transition as shown in figure 2. U_1=108 feet per second.

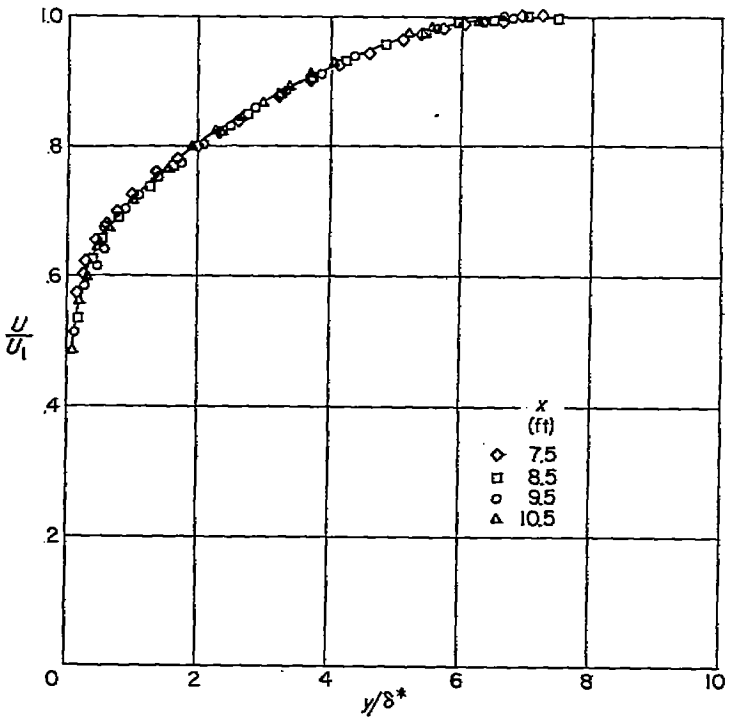

FIGURE 6.—Nondimensional mean-velocity distributions for free transition as shown in figure 2. U_1=108 feet per second.

At an angle of 5° the flow was no longer similar for the length of the plate. The use of screens seemed to be an effective method of thickening but was not further investigated because of the difficulties entailed in mounting a screen, keeping it under tension, and maintaining its shape for long periods of time.

Figures 13, 14, and 15 show the velocity distributions downstream from the distributed roughness at free-stream speeds of 35, 55, and 108 feet per second. Since the general characteristics for the three speeds are similar, the nondimensional profiles are given in figure 16 only for U_1=55 feet per second. It is seen that a distance of about 3.0 feet was required for similarity and that at x=10.5 feet the layer was approximately 3 inches thick, which for U_1=55 feet per second is the thickness of a layer having its beginning about 14 feet upstream. In other words, the virtual origin of the layer was displaced 3.5 feet upstream of the leading edge. There was some gain in effective distance at the higher speed. At U_1=108 feet per second, the virtual origin was about 5.5 feet upstream of the leading edge.

Comparison of the velocity distributions in the various artificially thickened layers is made with that of free transition, in figure 17, at approximately the same Reynolds number R_θ. The agreement is excellent. To test the universal character of the velocity distributions, it is of interest to compare them with those of other investigations. In figure 18, the distributions in the layer thickened by sand roughness are compared with the measurements of Hama (reference 11) and Schultz-Grunow (reference 12). The two curves show the effect of Reynolds number, and the data are sufficiently consistent to conclude that the velocity distributions obtained for the artificially thickened layer are characteristic of a turbulent boundary layer with zero pressure gradient and a smooth surface.

COMPARISON WITH LOGARITHMIC LAWS

Much of the theoretical work that has been done on the turbulent boundary layer is based on the application of the logarithmic laws of velocity distribution derived for flow in pipes and channels (reference 13). These involve the adoption of the mixing-length concept, a form for the shearing-stress distribution, and the omission of the influence of viscosity on the turbulence.

The wall-proximity law and the velocity-defect law for the velocity distribution are compared with experimental results in figures 19 and 20. The value of U_τ in the present measurements was determined from the measured velocity profile by means of the Von Kármán momentum equation which for zero pressure gradient gives

$$\frac{d\theta}{dx}=\frac{\tau_o}{2q_1}$$

The mean-velocity distributions for the artificially thickened turbulent boundary layer with zero pressure gradient, together with those of Schultz-Grunow (reference 12) and Freeman (reference 14), are plotted in the form of U/U_τ against yU_τ/ν in figure 19. In contrast with the measurements for pipes and channels, it is seen that there is a systematic increase in the deviation from the logarithmic law as the Reynolds number decreases. In the region where the law is valid figure 19 gives values of 4.2 for A and 5.75 for B. The following table gives the comparison with the measurements in smooth pipes and channels for wall proximity.

Investigator	Type	A	B
Nikuradse (reference 15)	Pipe	5.0	5.75
Nikuradse (reference 16)	Channel	5.0	5.75
Dönch (reference 17)	Channel	5.0	5.75
Laufer (reference 5)	Channel	7.2	5.75
Klebanoff and Diehl	Boundary-layer	4.2	5.75

The commonly used values for the experiments of Nikuradse in smooth pipes for points near the wall is 5.5 for B and 5.8 for A, but Millikan (reference 18) has shown that values of 5.75 and 5.0 are in closer agreement with the measurements. The broken line in figure 19 shows that the power law

$$\frac{U}{U_\tau}=8.16\left(\frac{yU_\tau}{\nu}\right)^{1/7}$$

is a good approximation for the higher Reynolds number R_θ=152,000 throughout most of the layer, but it should be remarked that at the lower Reynolds numbers the agreement was not so good. The distributions at lower Reynolds numbers, on a log-log basis, had a sinuous appearance which seemed to decrease with increasing Reynolds numbers.

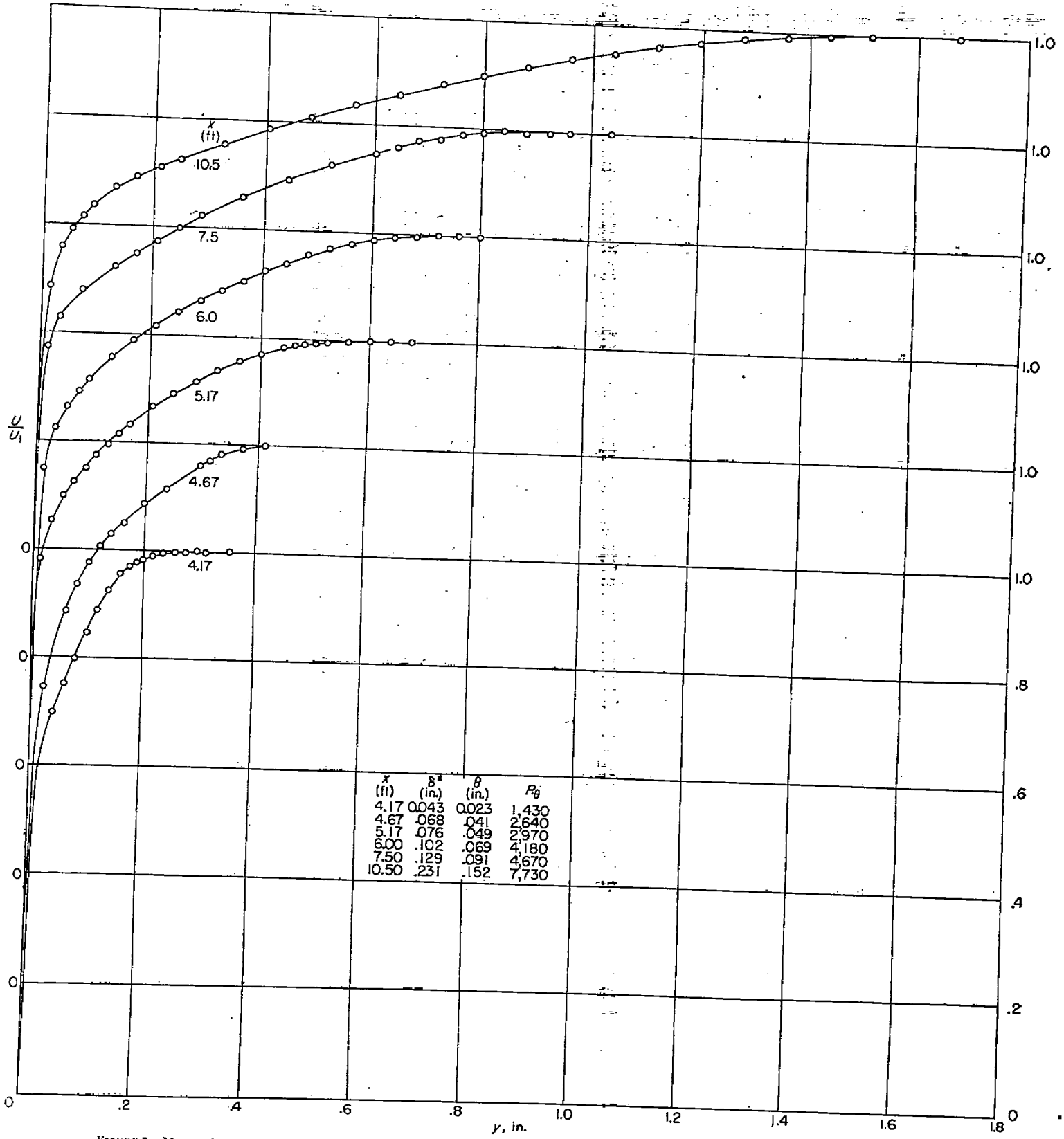

x (ft)	δ* (in.)	θ (in.)	R_θ
4.17	0.043	0.023	1,430
4.67	.068	.041	2,640
5.17	.076	.049	2,970
6.00	.102	.069	4,180
7.50	.129	.091	4,670
10.50	.231	.152	7,730

FIGURE 7.—Mean-velocity distributions for 0.04-inch cylindrical rod in contact with surface 4 feet from leading edge. U_1=108 feet per second.

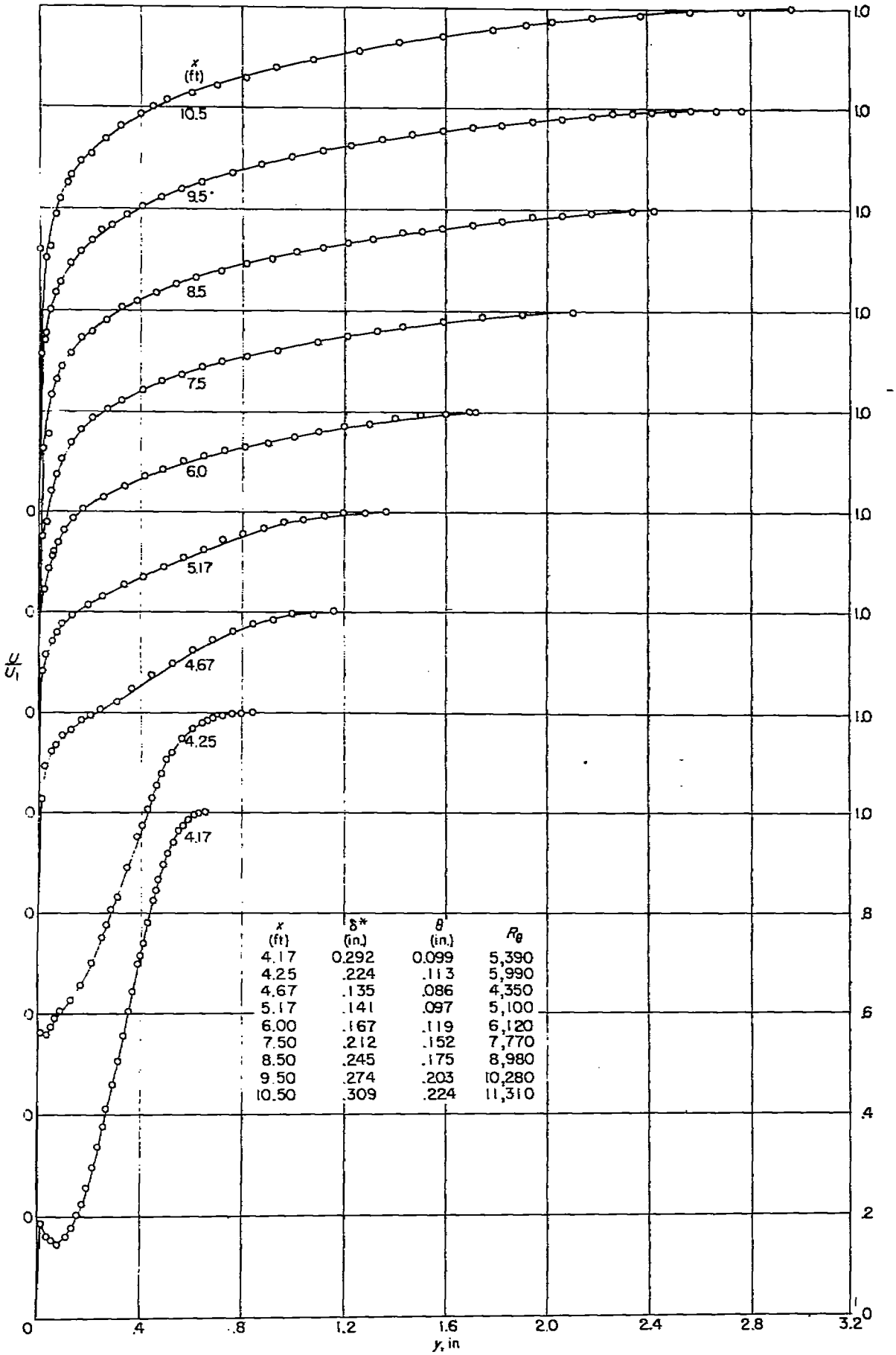

FIGURE 8.—Mean-velocity distributions for 0.25-inch cylindrical rod in contact with surface 4 feet from leading edge. U_1=108 feet per second.

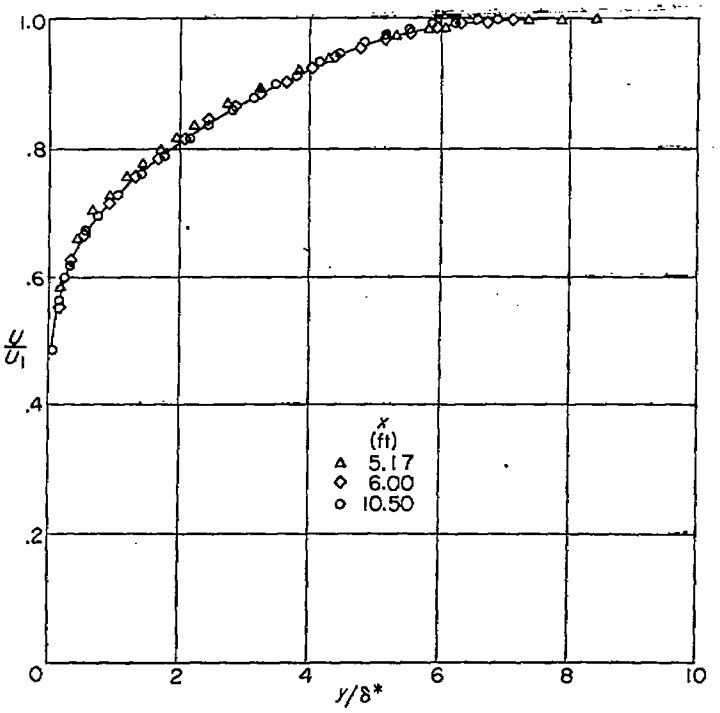

FIGURE 9.—Nondimensional mean-velocity distributions for 0.04-inch cylindrical rod in contact with surface 4 feet from leading edge. U_1=108 feet per second.

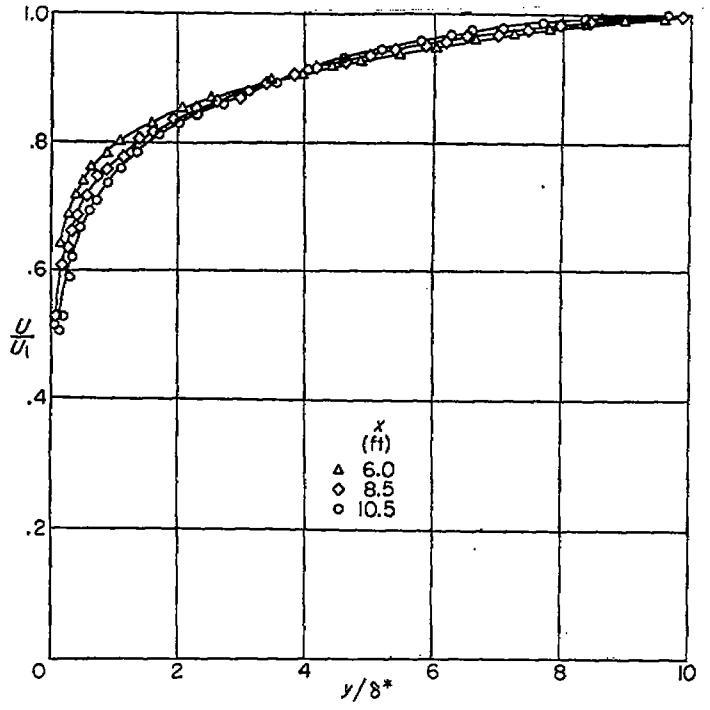

FIGURE 10.—Nondimensional mean-velocity distributions for 0.25-inch cylindrical rod in contact with surface 4 feet from leading edge. U_1=108 feet per second.

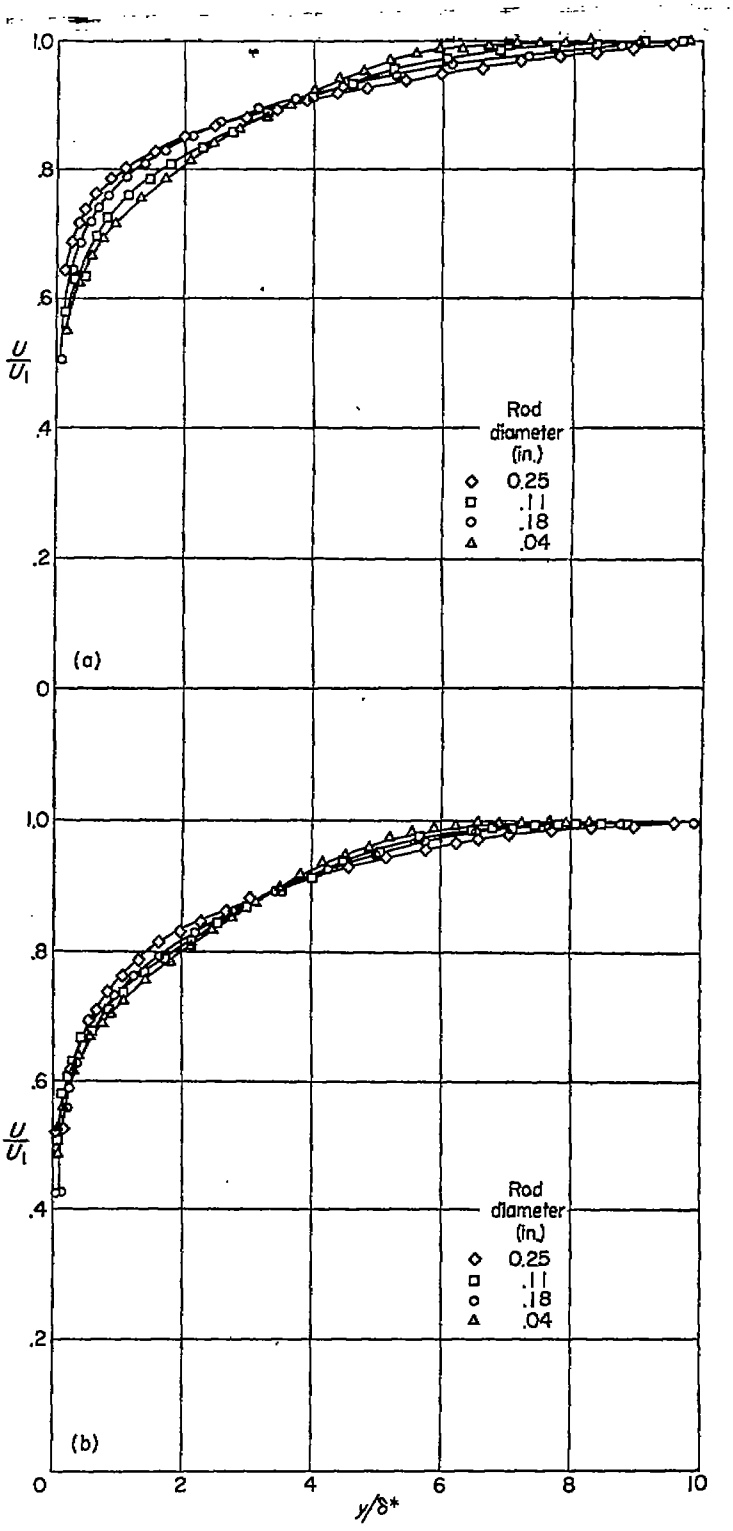

(a) x=6.0 feet.
(b) x=10.5 feet.

FIGURE 11.—Nondimensional mean-velocity distributions for various rod diameters. U_1=108 feet per second.

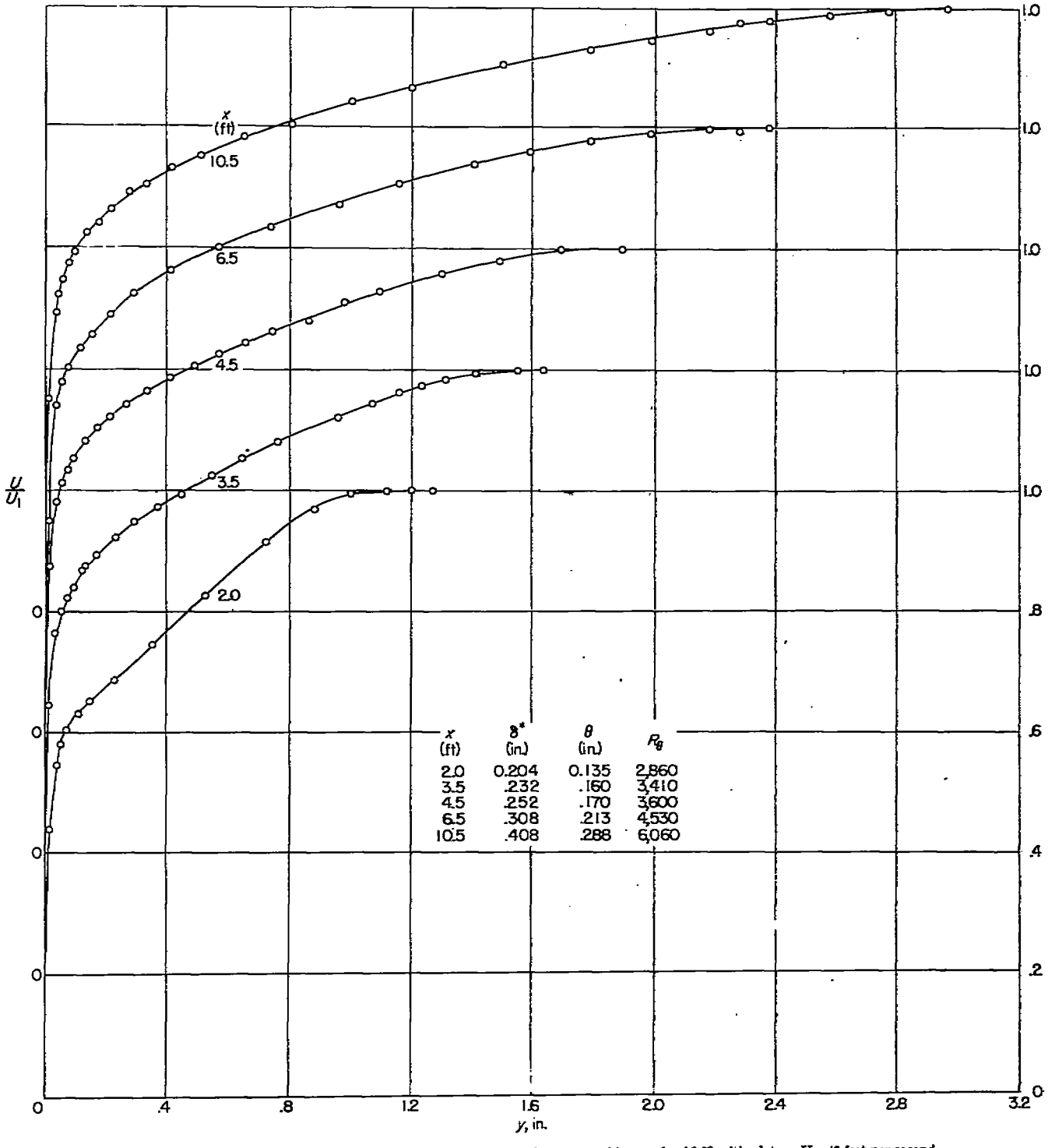

FIGURE 12.—Mean-velocity distributions for 1-foot span of 24-mesh screen making angle of 0.5° with plate. U_1=43 feet per second.

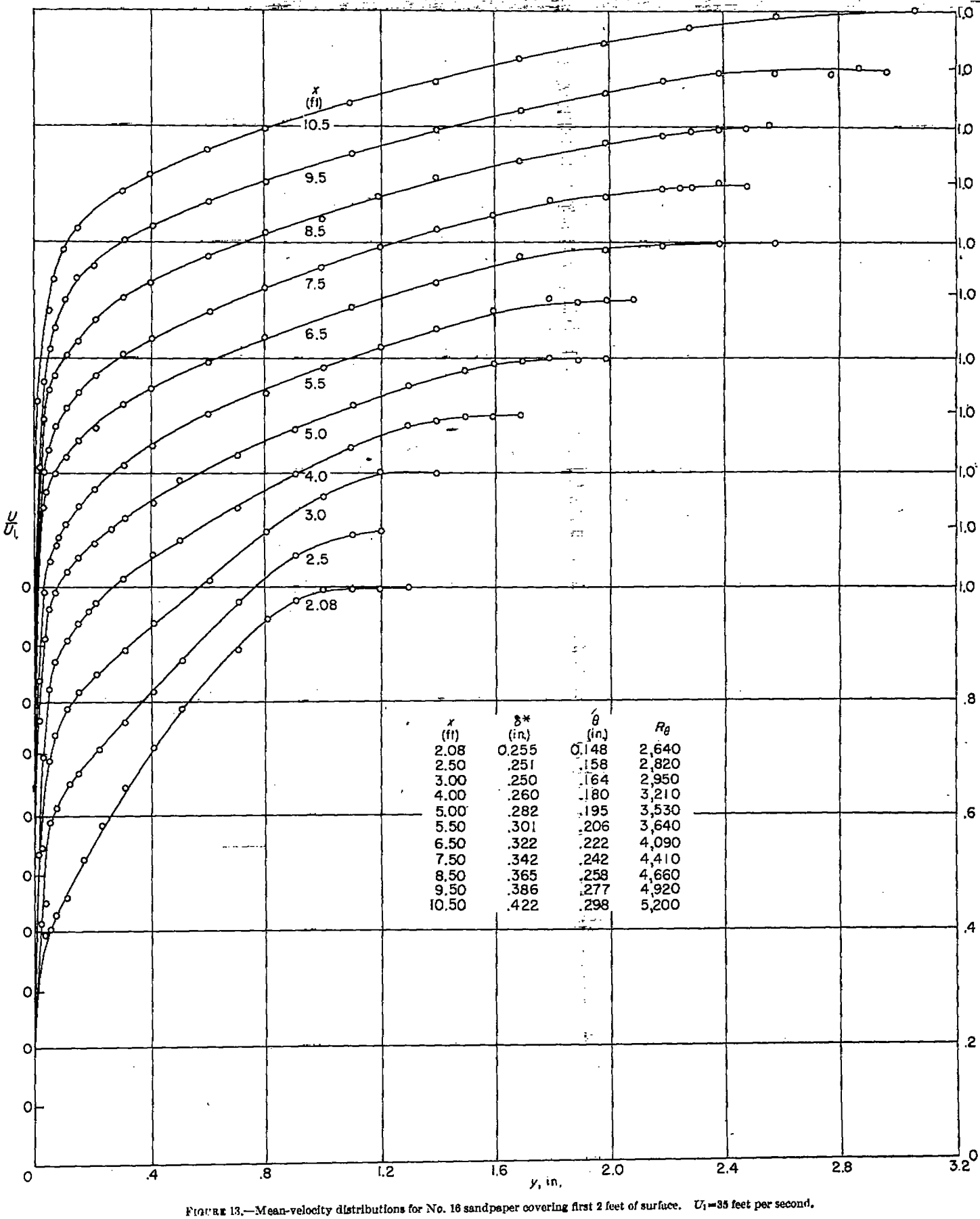

x (ft)	δ* (in.)	θ (in.)	R_θ
2.08	0.255	0.148	2,640
2.50	.251	.158	2,820
3.00	.250	.164	2,950
4.00	.260	.180	3,210
5.00	.282	.195	3,530
5.50	.301	.206	3,640
6.50	.322	.222	4,090
7.50	.342	.242	4,410
8.50	.365	.258	4,660
9.50	.386	.277	4,920
10.50	.422	.298	5,200

FIGURE 13.—Mean-velocity distributions for No. 16 sandpaper covering first 2 feet of surface. U_1=35 feet per second.

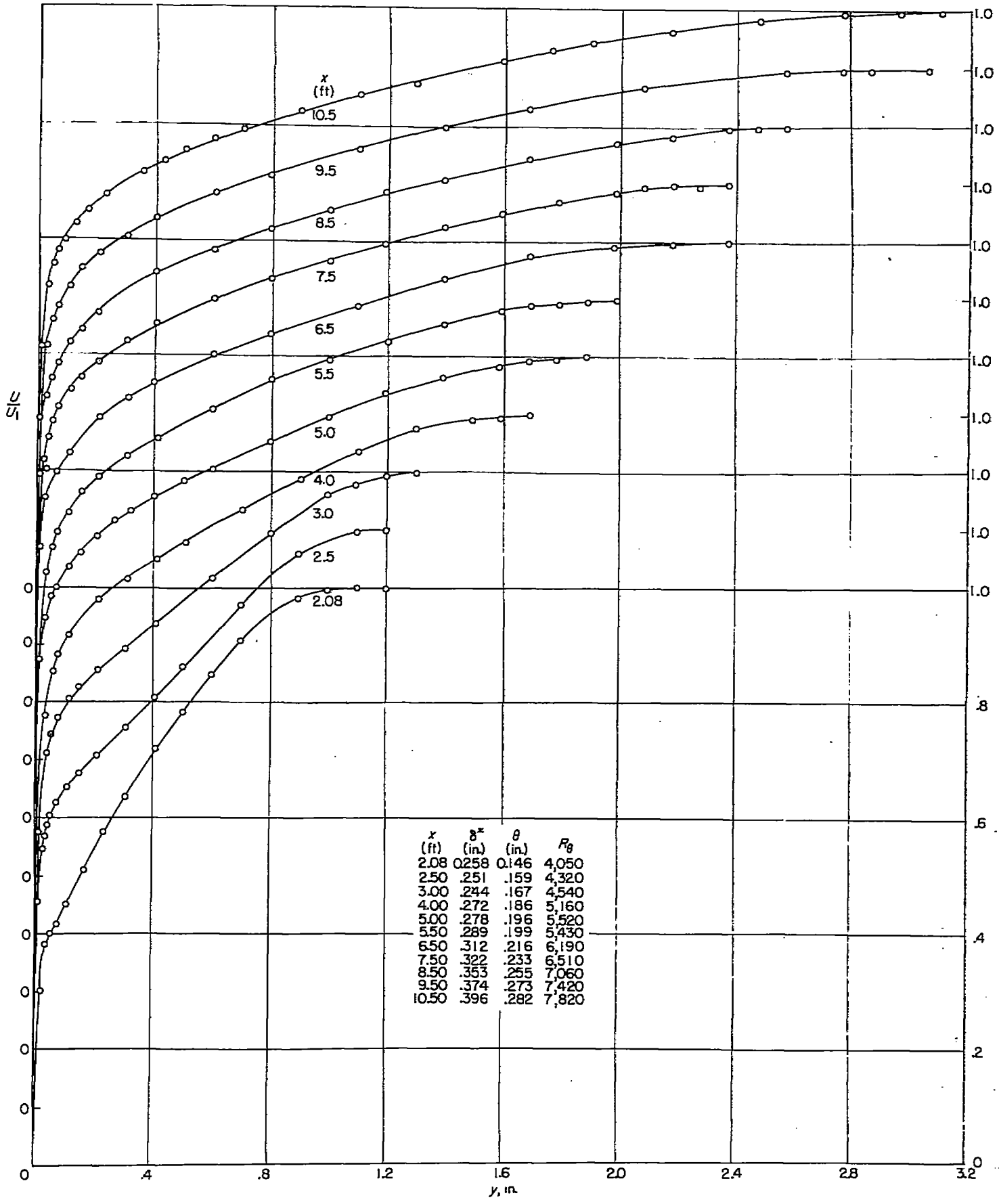

x (ft)	δ^* (in.)	θ (in.)	R_θ
2.08	0.258	0.146	4,050
2.50	.251	.159	4,320
3.00	.244	.167	4,540
4.00	.272	.186	5,160
5.00	.278	.196	5,520
5.50	.289	.199	5,430
6.50	.312	.216	6,190
7.50	.322	.233	6,510
8.50	.353	.255	7,060
9.50	.374	.273	7,420
10.50	.396	.282	7,820

FIGURE 14.—Mean-velocity distributions for No. 16 sandpaper covering first 2 feet of surface. U_1=55 feet per second.

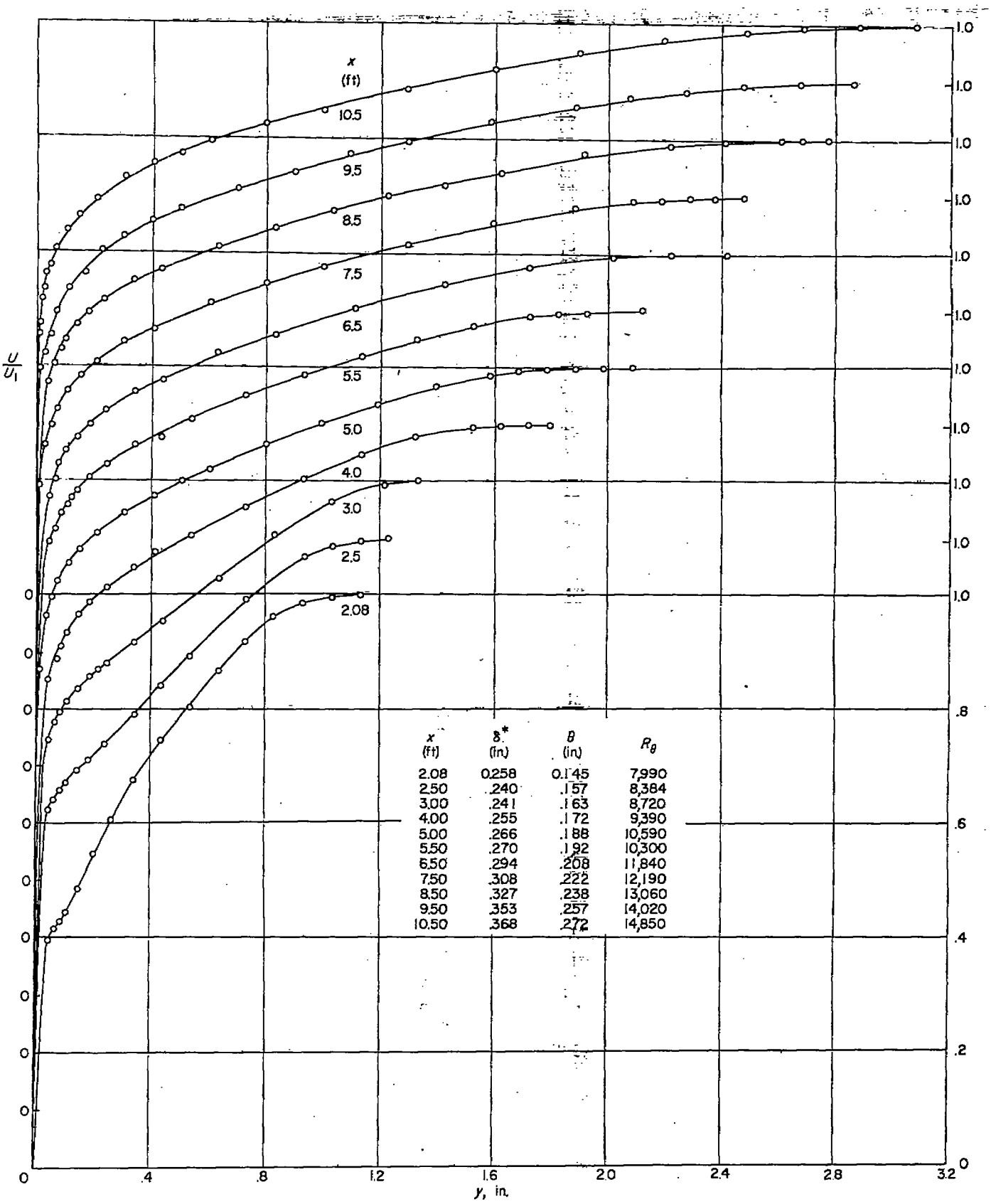

x (ft)	δ^* (in)	θ (in)	R_θ
2.08	0.258	0.145	7,990
2.50	.240	.157	8,384
3.00	.241	.163	8,720
4.00	.255	.172	9,390
5.00	.266	.188	10,590
5.50	.270	.192	10,300
6.50	.294	.208	11,840
7.50	.308	.222	12,190
8.50	.327	.238	13,060
9.50	.353	.257	14,020
10.50	.368	.272	14,850

FIGURE 15.—Mean-velocity distributions for No. 16 sandpaper covering first 2 feet of surface. U_1=108 feet per second.

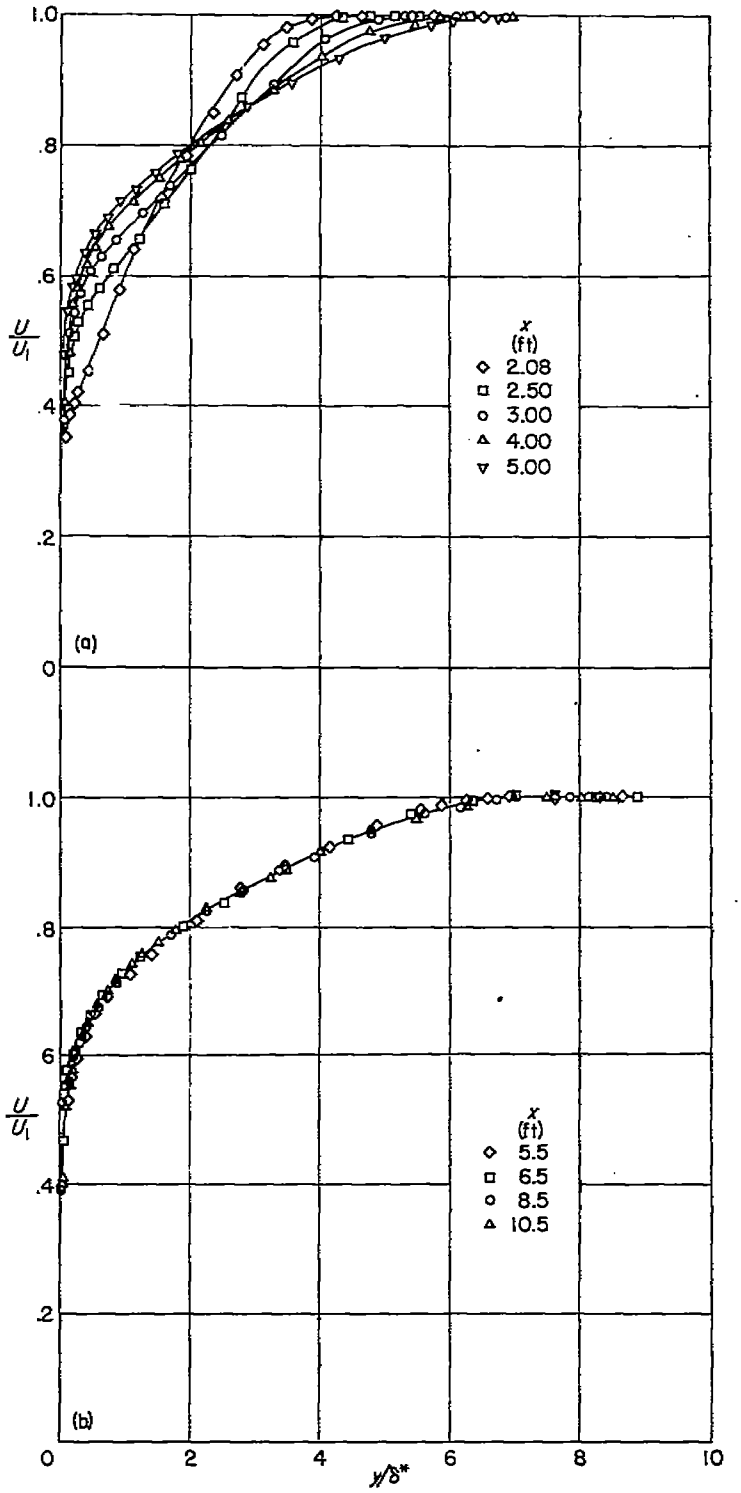

FIGURE 16.—Nondimensional mean-velocity distribution for No. 16 sandpaper covering first 2 feet of surface. U_1=55 feet per second.

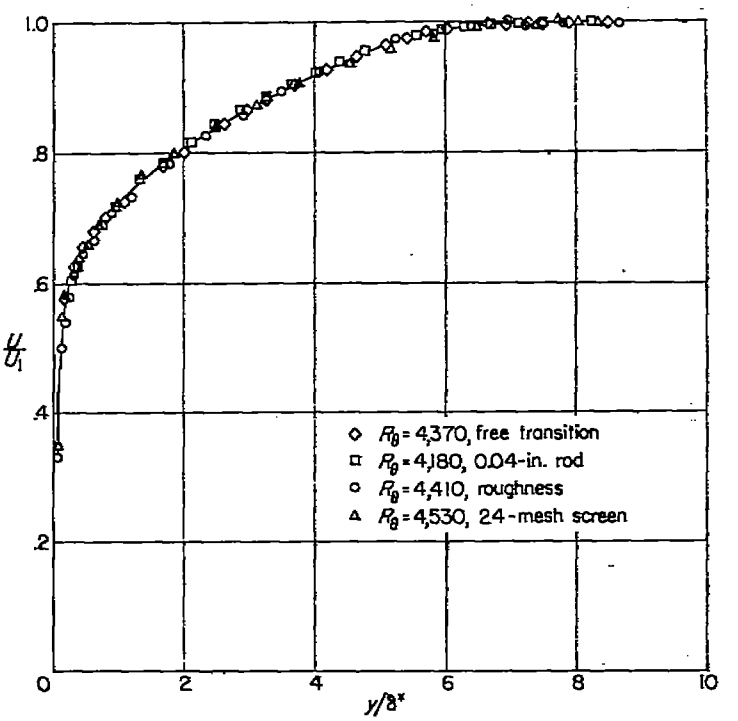

FIGURE 17.—Comparison of nondimensional mean-velocity distributions having approximately same values of R_θ.

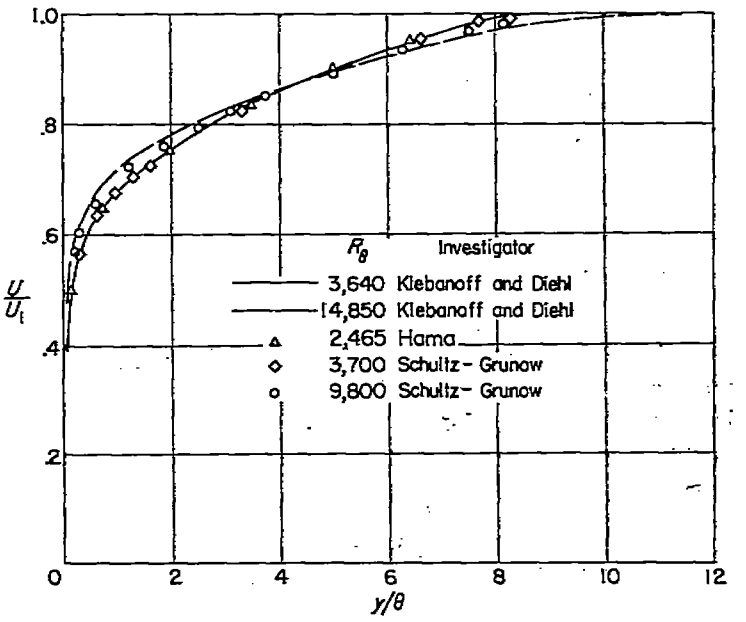

FIGURE 18.—Comparison of nondimensional mean-velocity distributions obtained by various investigators.

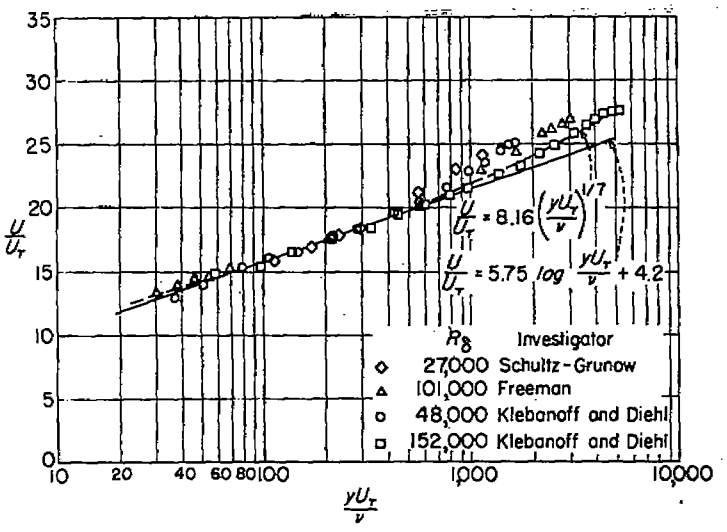

FIGURE 19.—Comparison of experimental results with 1/7-power law and logarithmic law.

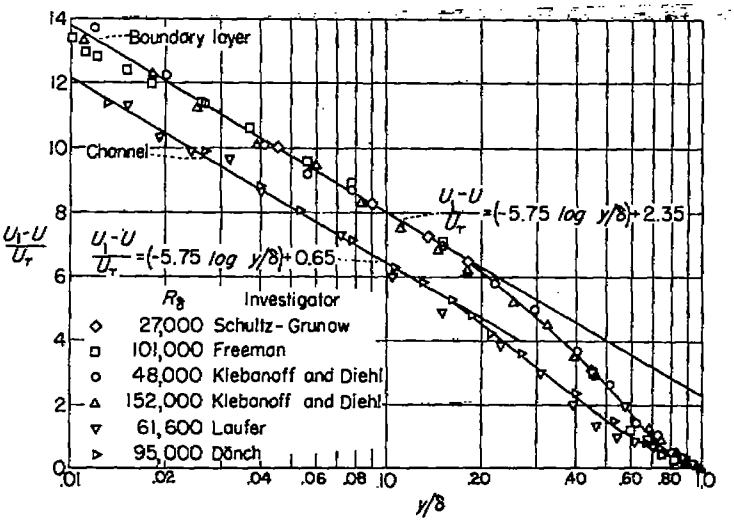

FIGURE 20.—Channel and boundary-layer profiles compared on basis of velocity-defect law.

In figure 20, both boundary-layer and channel results are plotted in the form suggested by the velocity-defect law. It is seen that results for both the boundary layer and the channel fit the straight lines up to $y/\delta=0.15$. The value of B seems to be universal for boundary layers and channels within this region. While results for pipes are omitted, it is remarked that the same holds true for pipe flow. It will be noted that the observed results are independent of Reynolds number when plotted in this way, indicating separate universal relationships of the form

$$\frac{U_1-U}{U_\tau}=f(y/\delta)$$

A point to be made with emphasis is that boundary-layer profiles are not like channel and pipe flow profiles, and it is seen that an artificially thickened boundary layer conforms to the pattern established in figures 19 and 20 after the similarity stage has been reached.

SPECTRUM AND INTENSITY OF u-FLUCTUATION

It has been shown in the previous section that, at a sufficient distance downstream, the mean-velocity distributions assume a universal character. However, the lack of knowledge concerning the relationship between the turbulence and the mean flow prohibits the use of mean-velocity distributions as direct evidence that the turbulence is fully developed. Since it is impractical to measure all the characteristics of the turbulence and in view of the interest in measurements of the spectrum in shear flow, the one-dimensional energy spectrum was chosen as the basis of comparison for the turbulence in the artificially thickened layers with that resulting from free transition.

The mean-square value of the u-fluctuations was measured between frequencies n and $n+dn$ at values of n from 10 to 10,000 cycles per second. Over most of the frequency range the accuracy of the spectrum measurements is within ± 10 percent. The accuracy was somewhat less at the low-frequency end below 100 cycles per second because of large-amplitude fluctuations and at the high end above 6000 cycles per second because of noise and possible wire-length effect. No wire-length corrections were made, and the noise level at 10,000 cycles per second was approximately 50 percent of the total signal. A direct over-all measurement of the intensity u'/U_1 was made during each spectrum determination to compare with that calculated from the spectrum and to serve as a check on the accuracy. In general, the agreement was within 5 percent. The spectrum curves are given in the nondimensional form $\frac{UF(n)}{L_x}$ against $\frac{nL_x}{U}$. Here $F(n)$ is the normalized spectrum function defined by

$$\int_0^\infty F(n)\,dn=1$$

and L_x is the integral scale defined by

$$L_x=\int_0^\infty R_x\,dx \tag{1}$$

where R_x is the longitudinal space correlation. The value of L_x was obtained from the intercept of the $F(n)$ curve at $n=0$ on the assumption that a space correlation was related to a time correlation by $x=Ut$ and using the Fourier transform written in the following form:

$$F(n)=\frac{4}{U}\int_0^\infty R_x \cos\frac{2\pi nx}{U}\,dx \tag{2}$$

From equations (1) and (2), when $n=0$

$$L_x=\frac{UF(n)_{n=0}}{4} \tag{3}$$

The values of L_x calculated by equation (3) for the turbulent boundary layer resulting from free transition and the boundary layers artificially thickened with a 0.04-inch rod and by roughness as described earlier are given in figures 21, 22, 23, and 24. It is noted that, except near the wall, L_x is constant across the layer and is proportional to the boundary-layer thickness, having a value of L_x/δ of approximately 0.4. It should be pointed out that the exactness of

equation (2) is open to question at high turbulence levels, since it requires that the fluctuations at a point be the result of a pure translation with velocity U of a fixed turbulence pattern.

For the condition of free transition, figure 21 shows a set of curves at $x=10.5$ feet, with $U_1=108$ feet per second, at different distances from the surface. It is seen that there is a systematic variation across the boundary layer up to $y/\delta=0.57$. Since L_x was used as the reference length, all curves are brought together at zero frequency. The trend in going toward the surface is for the higher frequencies (smaller eddies) to have proportionately more of the energy.

It may be that near the surface some of the smaller eddies can derive energy from the steep velocity gradient which exists and that farther away from the plate where the velocity gradient is comparatively small local isotropy begins at a lower wave number. It is hoped that future measurements of the spectrum of shearing stress will throw some light on this point.

Comparison is made in figure 22, at $x=10.5$ feet and $y/\delta=0.03$ and $y/\delta=0.57$, with the spectra obtained in the boundary layer resulting from free transition and those obtained in the artificially thickened layers using a 0.04-inch rod and sand roughness. The free-stream speed was 108 feet per second for the rod and free transition and 55 feet per second for the roughness so that the boundary-layer Reynolds number is approximately the same. The spectra are similar to one another and the same family of spectra exists in the artificially thickened layers as for that resulting from free transition.

Spectrum measurements made at various distances downstream from the 0.04-inch rod, at y/δ values of 0.57 and 0.4 and $U_1=108$ feet per second, are given in figure 23. It will be noted that the curves for $x=6.0$, 7.5, and 10.5 feet are similar. Although a single curve is drawn through the measured points, there is evidence of a Reynolds number effect in the downstream direction on the high-frequency end of the spectrum. The energy associated with the higher frequencies is so small that it does not distort the normalized curve at the low-frequency end. The curve for $x=4.17$ feet at $y/\delta=0.4$ which is only 2 inches from the rod is definitely dissimilar. This curve is practically flat up to 1500 cycles per second. The same characteristic flatness was also observed at $y/\delta=0.03$, so no particular significance should be attached to the value of $y/\delta=0.4$, as compared with the rest of the curves with $y/\delta=0.57$. Measurement of the spectrum for the condition of free transition, at $x=6.9$ feet, which was as close as it was possible to approach the transition because of the back-and-forth movement of transition, showed no evidence of the characteristic flatness observed close to the rod. In fact, it gave evidence that similarity of the spectra began at the downstream extreme of the transition region. In the case of free transition, the spectrum was also measured in the laminar layer at $x=4.5$ feet. A very sharp peak was found at 280 cycles per second, the predominant frequency of the laminar-boundary-layer oscillations, and little energy was found at other frequencies. There was no evidence of this peak in the turbulent boundary layer at $x=6.9$ feet. It was thought at first that the flatness of the spectrum observed near the rod was associated with the distorted mean-velocity profile and that here was evidence of a connection between turbulence distortion and mean-velocity distortion. However, figure 24, which pertains to thickening by roughness, shows no effect in the spectrum at the 3-foot position where the mean-velocity profile was definitely distorted. It would seem that the flatness of the spectrum measured near the rod is an effect peculiar to the rod and may be associated with eddy frequencies from the rod superimposed on a more or less normal spectrum.

It may be expected that, in the turbulent boundary layer, at a distance far enough away from the wall an extensive region of local isotropy exists. It is of interest to see how well the spectra in the artificially thickened turbulent boundary layer where the Reynolds number of turbulence is high agree with existing theories predicting the shape of the spectrum in isotropic turbulence.

Before making the comparison it may be well to discuss briefly some important features of the theory. A fundamental concept in the theories introduced by Kolmogoroff (references 1 and 2) and Heisenberg (reference 19) is that energy passes into the spectrum by way of the larger eddies and is then passed on to smaller and smaller eddies. Appreciable dissipation by viscosity starts only when the eddies get small enough. Beyond a certain wave number, smaller eddies get their energy only from larger eddies and are supplied sufficient energy to be kept in statistical equilibrium even in cases where the larger eddies are decaying. When the Reynolds number of turbulence $u'L_x/\nu$ is high, there will exist in the lower-wave-number part of the equilibrium range a subrange in which inertial forces predominate and the transfer of energy is equal to the total dissipation ϵ and at the high-wave-number end another subrange where viscous effects predominate. Heisenberg assumed that the transfer of energy at wave number k was caused by a turbulence friction produced by eddies with wave numbers greater than k and that the total dissipation involved a turbulence viscosity plus ordinary viscosity in an expression of the following form:

$$\epsilon=\left[\nu+\chi\int_k^\infty\sqrt{\frac{E(k'')}{(k'')^3}}\,dk''\right]\int_0^k 2(k')^2E(k')\,dk' \qquad (4)$$

Here the second term within the brackets represents the turbulence viscosity, and χ is an absolute constant. The solution of equation (4) gives the spectrum in the equilibrium range the form

$$E(k)=\left(\frac{8\epsilon}{9\chi}\right)^{2/3}k^{-5/3}\left[1+\left(\frac{k}{k_s}\right)^4\right]^{-4/3} \qquad (5)$$

where k_s is a wave number in the intermediate range where inertial forces and viscosity both play a role and is given by

$$k_s=\left(\frac{3\chi^2\epsilon}{8\nu^3}\right)^{1/4}$$

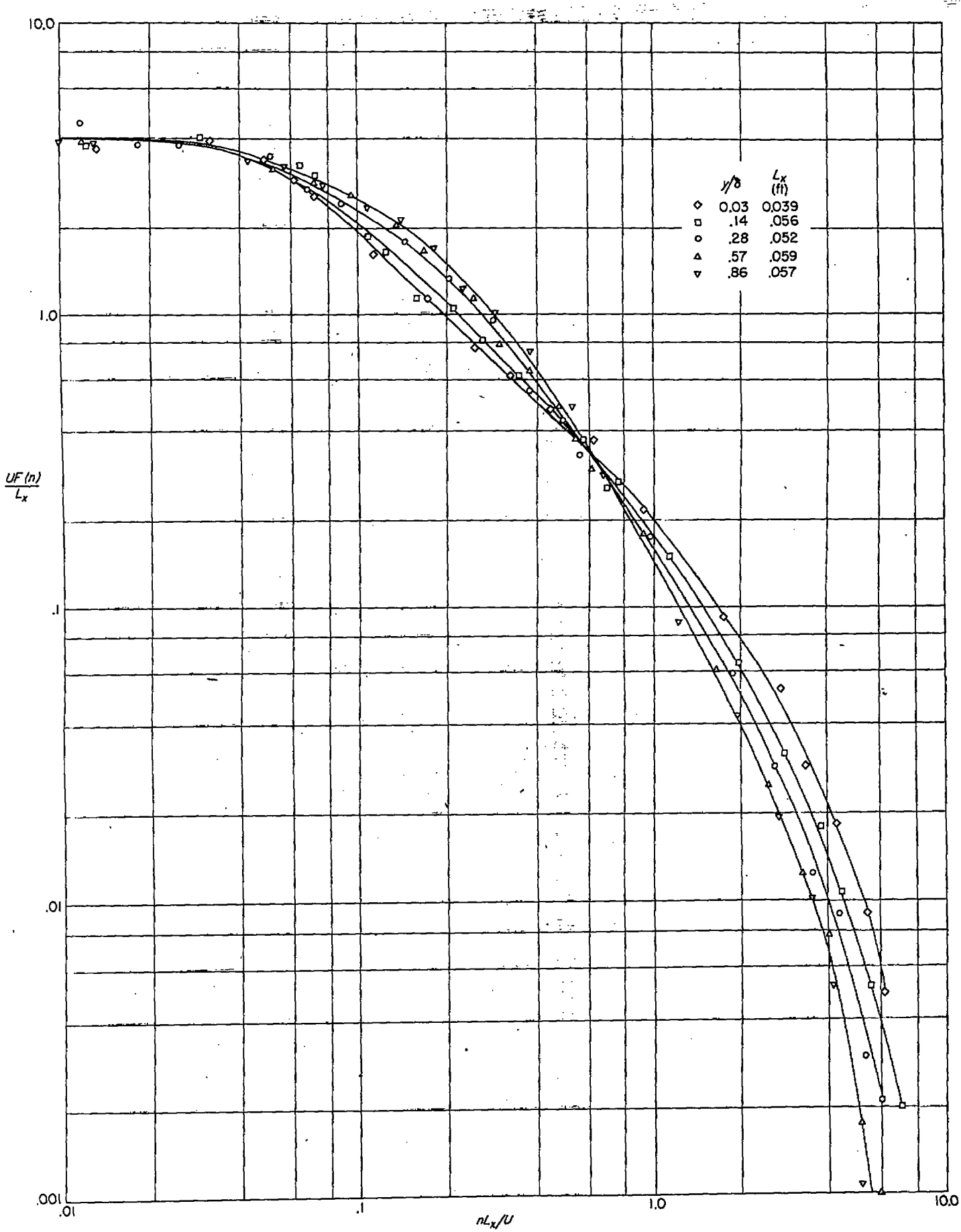

FIGURE 21.—Spectrum of u-fluctuations in turbulent boundary layer resulting from free transition. $x=10.5$ feet; $U_1=108$ feet per second.

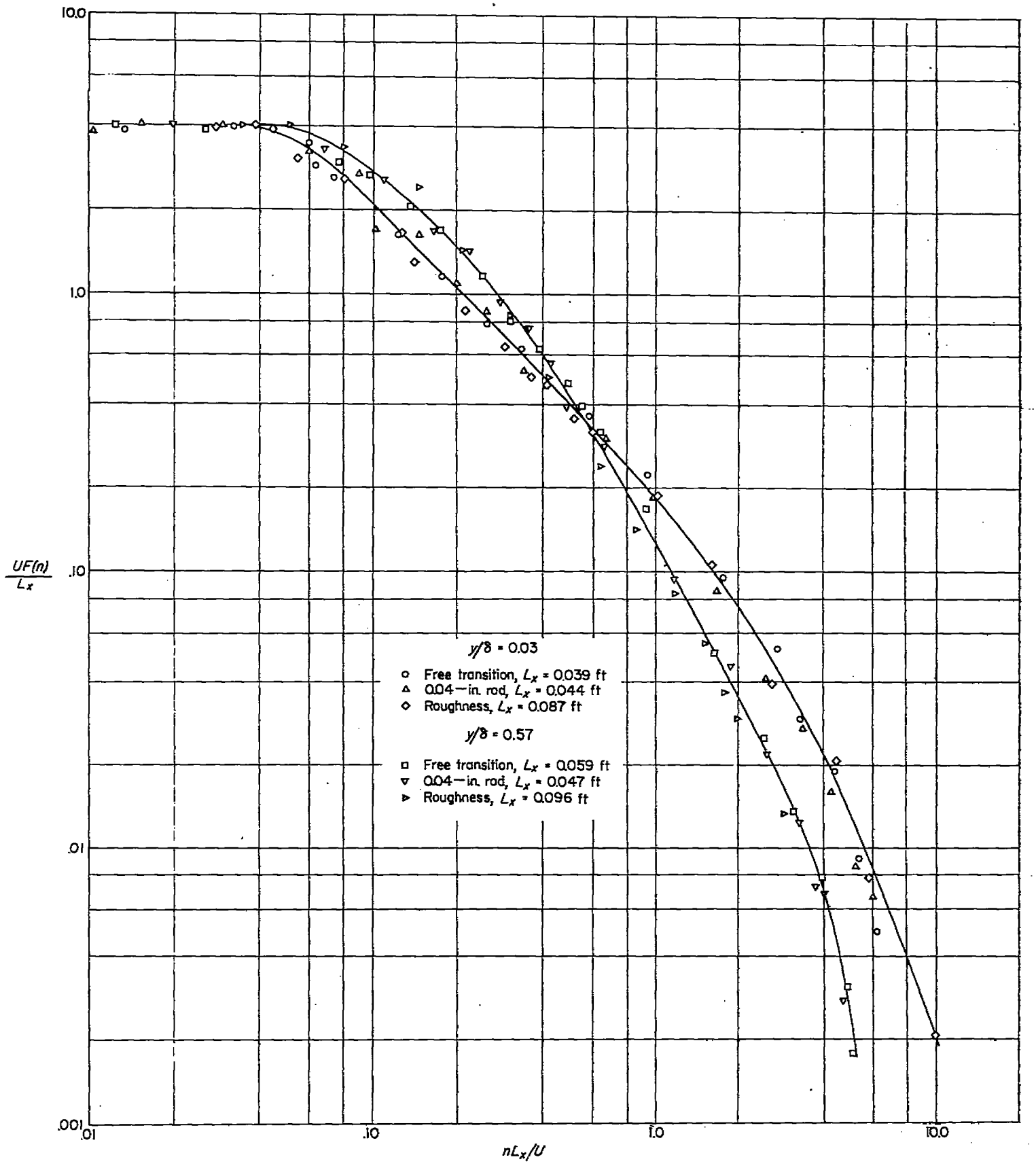

FIGURE 22.—Spectrum of u-fluctuations in turbulent boundary layer at x=10.5 feet. U_1=108 feet per second for free transition and 0.04-inch rod; U_1=55 feet per second for roughness.

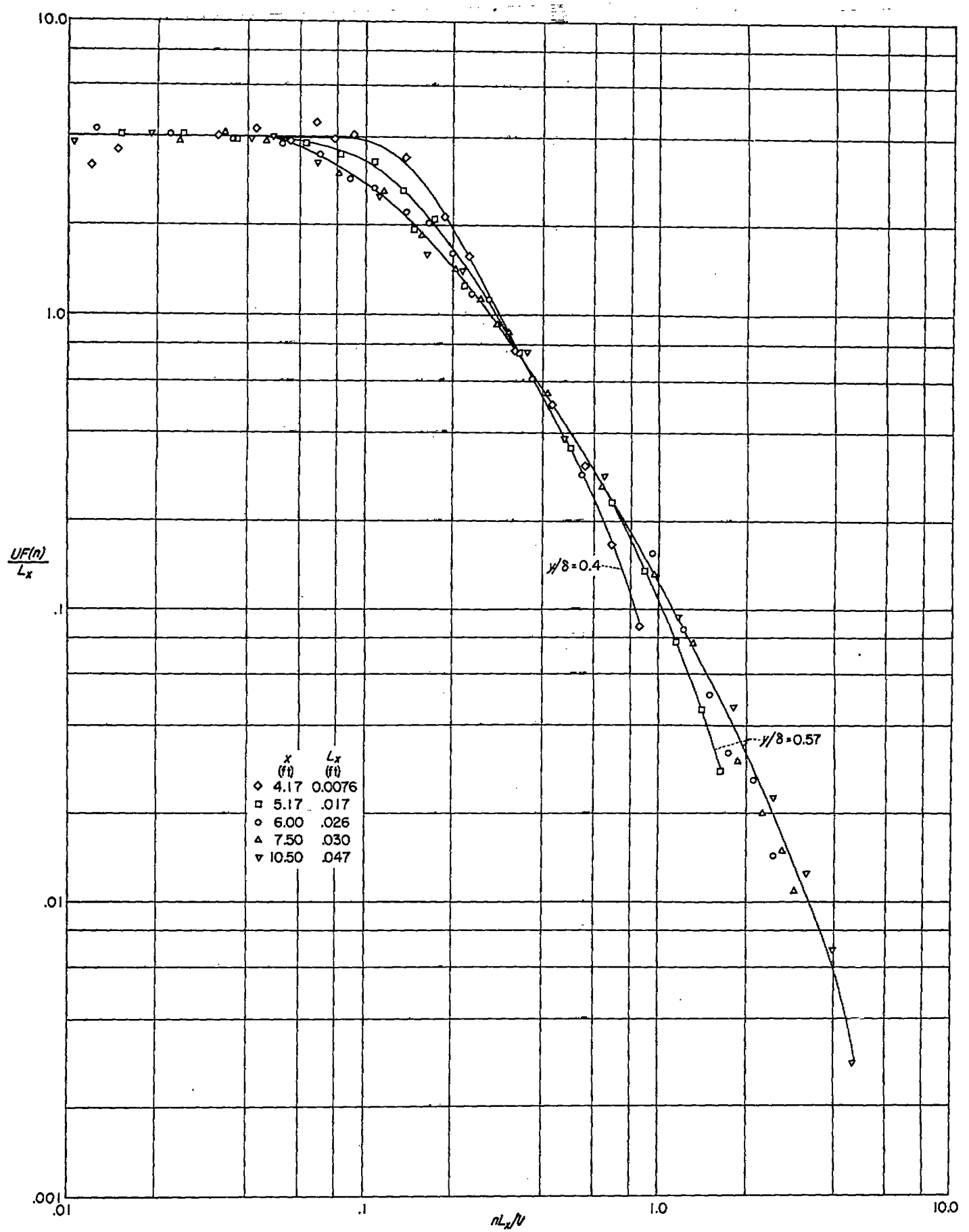

FIGURE 23.—Spectrum of u-fluctuations in turbulent boundary layer for 0.04-inch rod in contact with surface 4 feet from leading edge. U_1=108 feet per second.

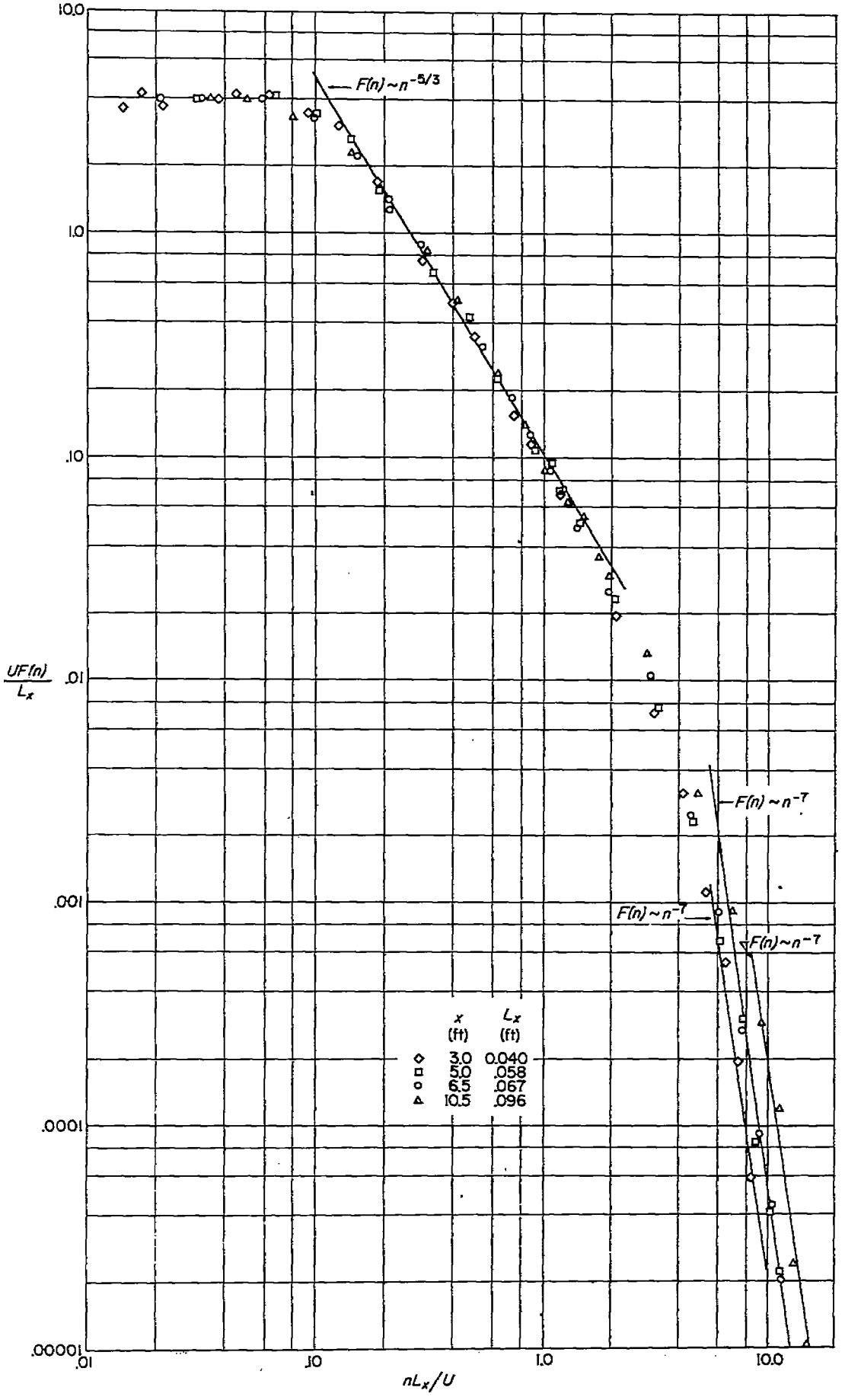

FIGURE 24.—Test of −5/3 law and −7 law for spectrum of u-fluctuations in turbulent boundary layer thickened by roughness for first 2 feet of surface. U_1=55 feet per second; y/δ=0.57.

The equilibrium spectrum given by equation (5) deals with a three-dimensional energy spectrum. In order to compare with experiment it is necessary to transform this equation to the one-dimensional form using the following relationship also derived by Heisenberg:

$$E_x(k_x)=\frac{1}{4}\int_{k_x}^{\infty}\frac{E(k)}{k^3}(k^2-k_x^2)dk \tag{6}$$

The one-dimensional form of equation (5) is found to be

$$E_x(k_x)=\frac{9}{110}A_1k_x^{-5/3}\left[1+\left(\frac{k_x}{k_{sx}}\right)^4\right]^{-4/3} \tag{7}$$

where

$$A_1=\left(\frac{8\epsilon}{9\chi}\right)^{2/3}$$

and

$$k_{sx}=0.645\,k_s$$

In the inertial range, that is, $k_x \ll k_{sx}$, equation (7) becomes

$$E_x(k_x)=\frac{9}{110}A_1k_x^{-5/3} \tag{8}$$

and in the viscous range, that is, $k_x \gg k_s$, equation (7) becomes

$$E_x(k_x)=\frac{1}{126}A_2k_x^{-7} \tag{9}$$

where

$$A_2=\left(\frac{\chi\epsilon}{2\nu^2}\right)^2$$

In figure 24, equations (8) and (9) are compared with the spectra measured at different distances downstream from the roughness, at $y/\delta=0.57$ and $U_1=55$ feet per second. At the high-turbulence Reynolds number of the boundary layer, the existence of a $-5/3$ region is quite evident. The agreement with the n^{-7} law should be taken with some reservation because of the lesser accuracy of the measurements at the high-frequency end of the spectrum. It should be mentioned in passing that the slope of the spectrum curves at $y/\delta=0.03$, such as shown in figure 22, is approximately 1, where the $-5/3$ region exists at $y/\delta=0.57$.

It is seen from figure 25 that in the intermediate range of frequencies equation (7) does not agree so well as the interpolation formula

$$E_x(k_x)=\frac{9}{110}A_1k_x^{-5/3}\left[1+\left(\frac{k_x}{k_{sx}}\right)^{8/3}\right]^{-2} \tag{10}$$

suggested by Heisenberg. For convenience, equations (7) and (10) are represented in figure 25 as

$$F(z)=A_o\left(\frac{z}{z_s}\right)^{-5/3}\left[1+\left(\frac{z}{z_s}\right)^4\right]^{-4/3} \tag{7a}$$

and

$$F(z)=A_o\left(\frac{z}{z_s}\right)^{-5/3}\left[1+\left(\frac{z}{z_s}\right)^{8/3}\right]^{-2} \tag{10a}$$

where

$$F(z)=\frac{UF(n)}{L_x}$$

and

$$z=\frac{nL_x}{U}$$

and A_o and z_s are experimentally determined. Formula (10a), as shown in figure 26, is also in good agreement with some unpublished measurements made in isotropic turbulence 50 inches downstream from a 1-inch grid in the NBS 4½-foot wind tunnel. The fact that the analytical relation (7) does not agree with the measured spectra so well as the empirical expression (10) would indicate that equation (4) may not yet be quite exact. Expressions (7a) and (10a) are identical in the extreme regions of the equilibrium range, and it is of interest to calculate the value of χ from the constants A_o and z_s. Since A_o and z_s are determined from a nondimensional normalized representation they are connected to χ by the following relations.

The term $E(k)$ of the three-dimensional spectrum is defined such that

$$\int_0^{\infty}E(k)\,dk=\frac{\overline{u^2}+\overline{v^2}+\overline{w^2}}{2}$$

From relation (6), it can be shown that

$$\int^{\infty}E_x(k_x)\,dk_x=\frac{1}{6}\int_0^{\infty}E(k)\,dk$$

so that, for isotropic turbulence where $\overline{u^2}=\overline{v^2}=\overline{w^2}$,

$$\int_0^{\infty}E_x(k_x)\,dk_x=\frac{\overline{u^2}}{4}$$

and

$$\frac{\overline{u^2}}{4}\int_0^{\infty}F(z)\,dz=\int_0^{\infty}E_x(k_x)\,dk_x$$

since

$$k_x=\frac{2\pi n}{U}=\frac{2\pi z}{L_x}$$

$$\frac{\overline{u^2}}{4}\frac{L_x}{2\pi}F(z)=E_x(k_x)$$

In the inertial range,

$$F(z)=A_oz_s^{5/3}z^{-5/3}$$

$$E_x(k_x)=A_oz_s^{5/3}L_x\overline{u^2}\frac{1}{8\pi}\left(\frac{2\pi}{L_x}\right)^{5/3}k_x^{-5/3}$$

and

$$\left(\frac{8\epsilon}{9\chi}\right)^{2/3}=A_1=\frac{110}{9}A_oz_s^{5/3}L_x\overline{u^2}\frac{1}{8\pi}\left(\frac{2\pi}{L_x}\right)^{5/3} \tag{11}$$

It will be noted that ϵ and $\overline{u^2}$ must be determined in addition to the quantities already mentioned before χ can be calculated by equation (11). For isotropic turbulence, the expression for the dissipation (reference 20) is

$$\epsilon=15\nu\frac{\overline{u^2}}{\lambda^2} \tag{12}$$

where λ is the microscale obtainable from a spectrum measurement by

$$\frac{1}{\lambda^2}=\frac{4\pi^2}{U^2}\int_0^{\infty}n^2F(n)\,dn \tag{13}$$

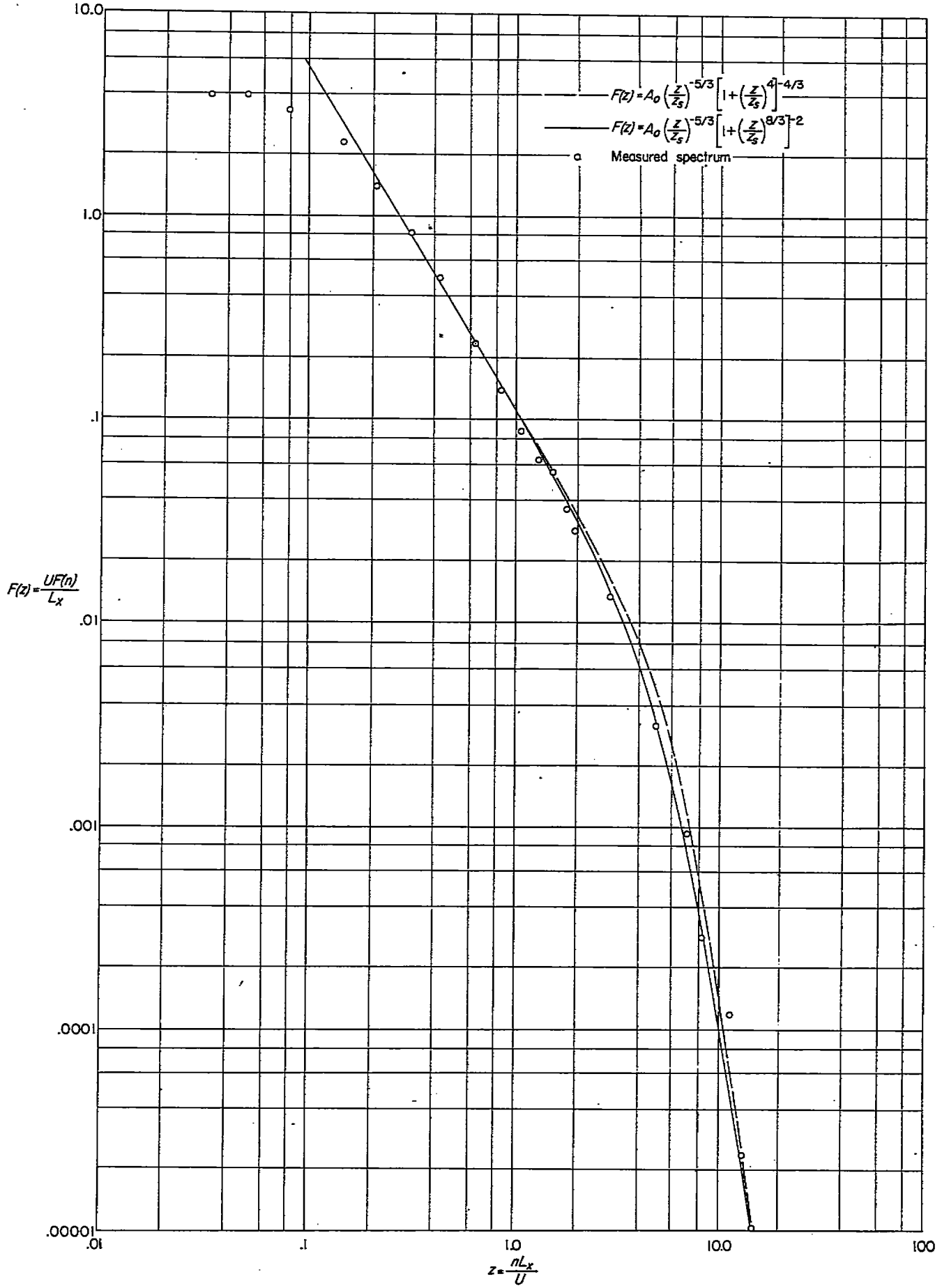

FIGURE 25.—Comparison of measured spectrum of u-fluctuations with Heisenberg's theoretical formula (broken line) and interpolation formula (solid line). Boundary layer thickened by No. 16 sandpaper for first 2 feet of surface. $x=10.5$ feet; $U_1=55$ feet per second; $A_0=5.29\times10^{-3}$; $z_s=6.15$.

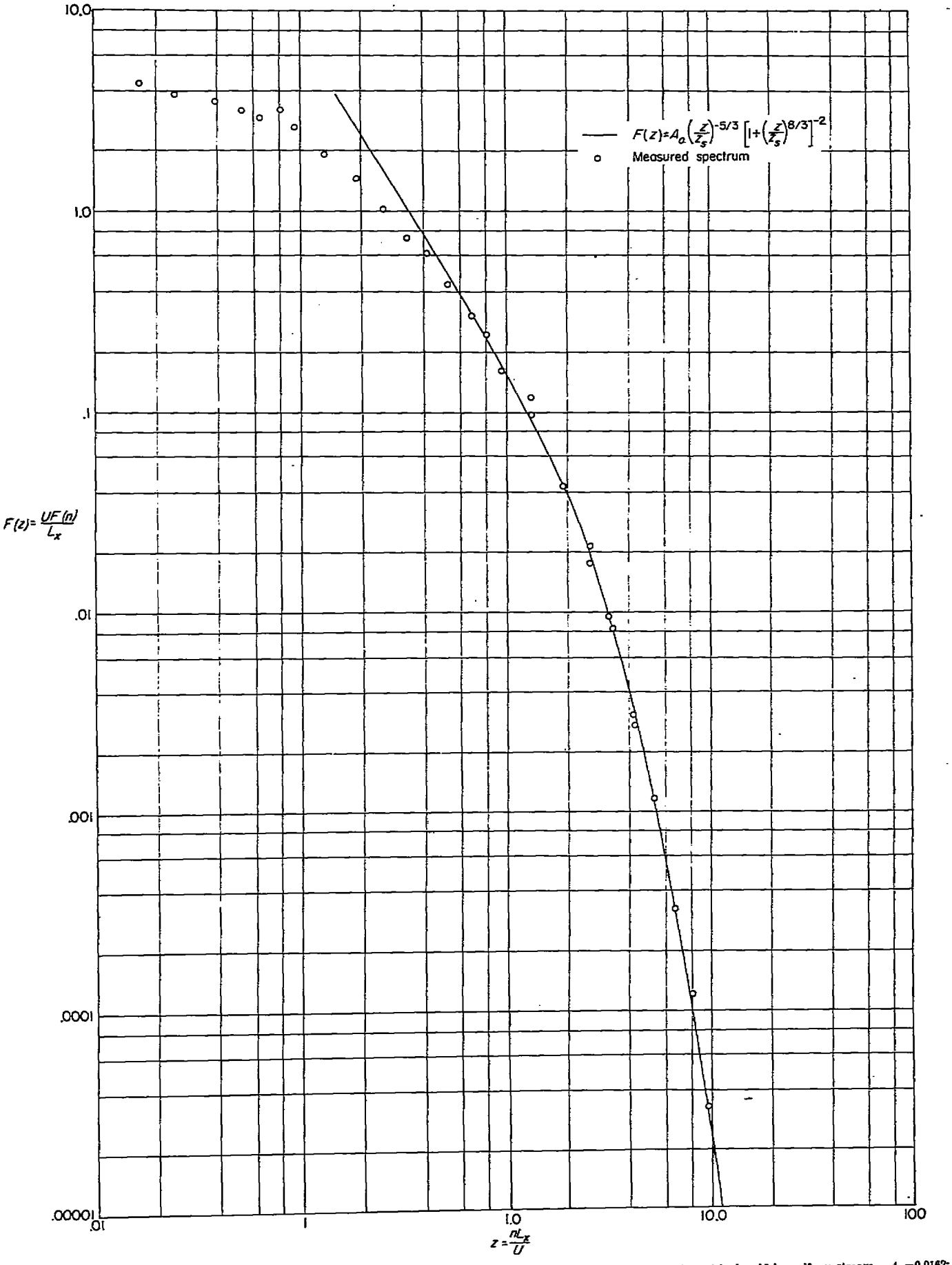

FIGURE 26.—Spectrum of isotropic turbulence compared with Heisenberg's interpolation formula. Measurements made 50 inches from 1-inch grid in uniform stream. $A_0=0.0162$; $z_s=4.00$ $u'/U=0.013$; $U=50$ feet per second; $L_x=0.047$ foot; and $\lambda=0.010$ foot

Partial justification for the use of such relationships where the turbulence does not have general isotropy is afforded by figure 27, where it is seen that about 90 percent of the integral in equation (13) is contributed by frequencies above 500 cycles per second. This is in the region where the $-5/3$- and -7-power laws hold and is therefore the region of local isotropy. It is concluded therefore as a reasonable approximation that λ determined by equation (13) is the appropriate and only scale entering into the viscous dissipation. However, much of the value of $\overline{u^2}$ is contributed below 500 cycles per second, and the assumption that $\overline{u^2}+\overline{v^2}+\overline{w^2}$ equals $3\overline{u^2}$, as made in equation (12), is not a sufficiently good approximation. Since $\overline{v^2}$ and $\overline{w^2}$ were not measured, the results of reference 6 were used to obtain

$$\overline{u^2}+\overline{v^2}+\overline{w^2}=0.62(3\overline{u^2})$$

at $y/\delta=0.57$. The factor 0.62 is applied to the right side of equation (12) and to equation (11) where $\overline{u^2}$ appears.

The value of χ calculated from equation (11) for the turbulent boundary layer artificially thickened by sand roughness, at $x=10.5$ feet and $y/\delta=0.57$, with the values of A_0 and z_s given in figure 25, is 0.23. The value of χ calculated for the case of isotropic turbulence shown in figure 26 is 0.65. By a similar procedure χ was calculated for the spectrum measured by Laufer in fully developed channel flow (reference 5), and a value of 0.52 was obtained. At present there are insufficient experimental data to determine the reason for the variations obtained. It is of interest to mention that the turbulence Reynolds numbers $\frac{u'L_x}{\nu}$ were 1790, 550, and 190 for the boundary layer, channel, and isotropic turbulence, respectively, and that corresponding increasing values of χ were obtained.

The insensitivity of the spectrum to distortions in the mean-velocity distributions as illustrated by figure 24 made it desirable to check further on the fully developed nature of the turbulence in the artificially thickened layer by measuring the distribution of u'/U_1. Intensity measurements were made at various distances downstream from the roughness at $U_1=108$ feet per second, and these are given in figure 28. At $x=3.0$ feet, 1 foot downstream from the

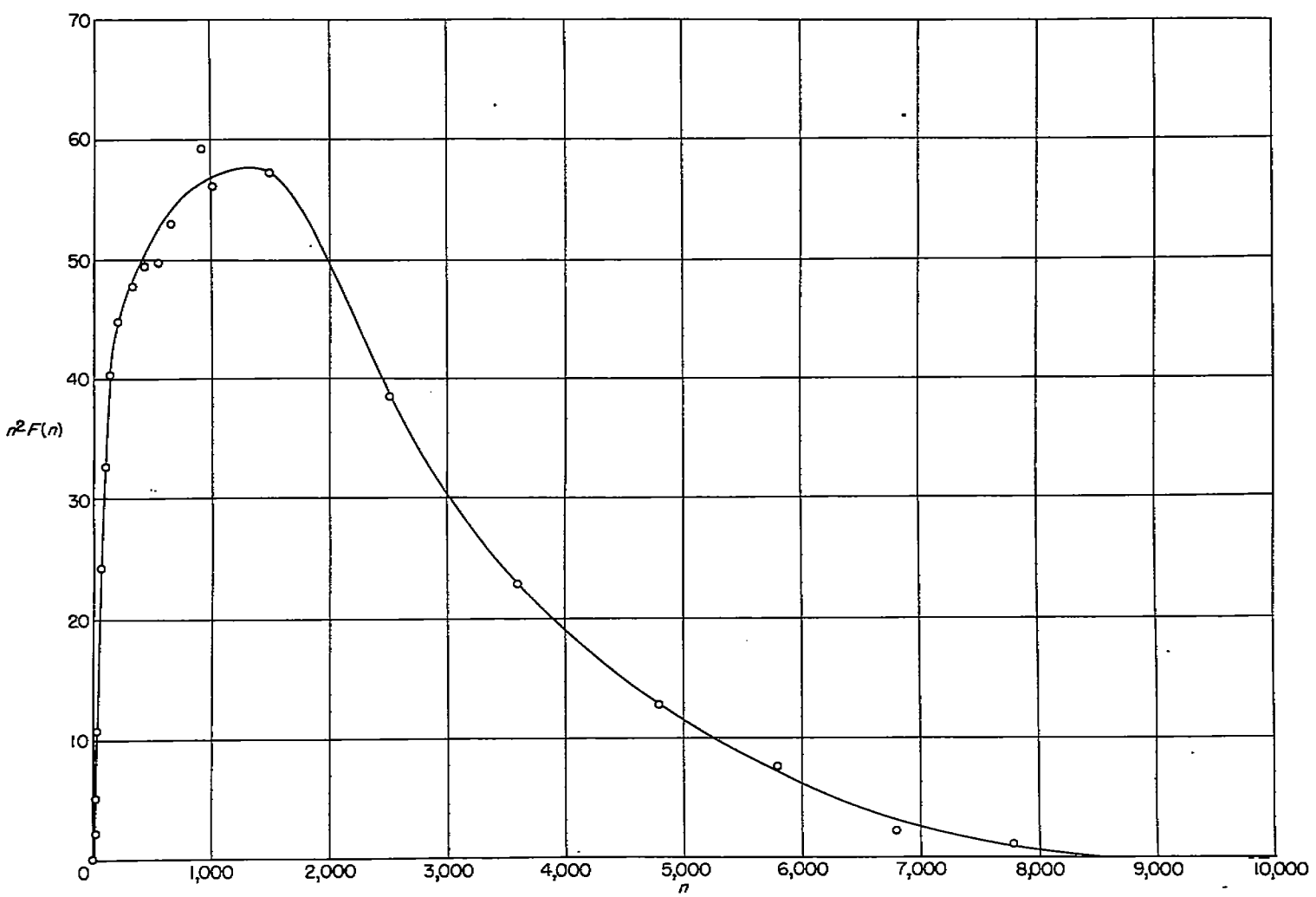

FIGURE 27.—Second moment spectrum curve used to obtain λ by formula (21).

edge of the roughness, the intensity is flat up to $y/\delta=0.4$ and is apparently the result of the diffusion of the high turbulence generated by the roughness. From $x=5.0$ to $x=10.5$ feet, the distributions of u' exhibit similarity, which is the same region for which the mean-velocity distributions were similar. The change in turbulence level accompanying a change in speed from 108 to 55 feet per second is also shown. It should be noted that there is no change in level accompanying the variations in boundary-layer Reynolds number due to changes in boundary-layer thickness.

An interesting feature of the turbulence in the boundary layer was its intermittent nature in the outer portions of the layer. This was also observed by Townsend for a wake (reference 21) and by Corrsin for a turbulent jet (reference 22). It seems to be characteristic of shear flow with a free boundary. Figure 29 shows two oscillograms taken at $x=10.5$ feet, at $y/\delta=0.03$ and $y/\delta=0.75$. At $y/\delta=0.03$ there

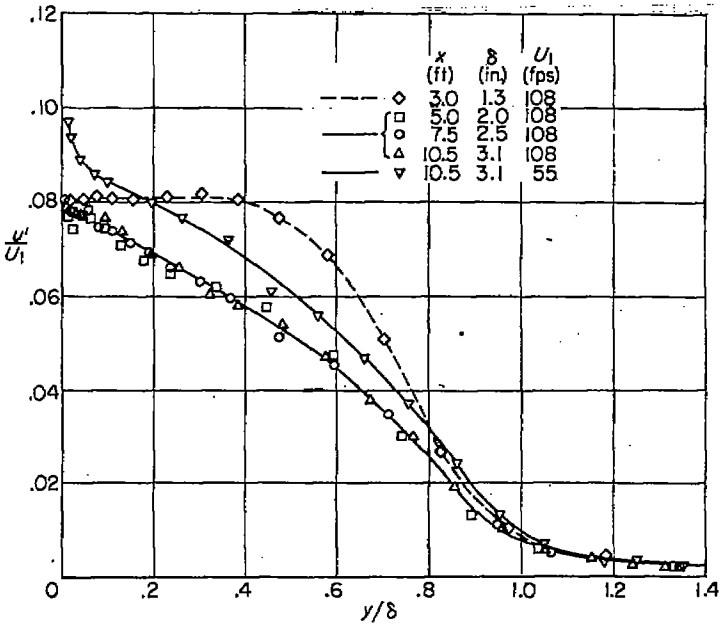

FIGURE 28.—Intensity of u-component of turbulence for boundary layer thickened by No. 16 sandpaper over first 2 feet of surface.

is no trace of intermittency, while at $y/\delta=0.75$ it is quite marked. Observation of the oscilloscope trace indicated there is a gradual increase in the intermittency as the distance from the surface increased. It is planned in the future to make some quantitative measurements of the intermittency and its effect on the measured turbulence intensity

CONCLUSIONS

From tests made to determine the feasibility of artificially thickening a turbulent boundary layer on a flat plate, the following conclusions can be drawn:

1. It has been established that by artificial methods it is possible to thicken substantially a fully developed turbulent boundary layer on a flat plate. The layer so formed becomes characteristic of that developed from the beginning on a smooth flat plate after passing over the required length of smooth surface. For a given boundary-layer thickness, artificial thickening makes possible a saving in length provided that there is enough length for the layer to become free from distortions.

2. Almost any kind of obstruction placed on the surface would produce a thickened turbulent flow, but only from a certain class did downstream effects disappear in a reasonably short distance. This class appeared to be characterized by the ability to absorb energy from the mean flow without introducing large-scale disturbance. Two examples of this class are as follows:

(1) A fine-mesh screen placed so that the plate and screen form a narrow wedge opening into the wind

(2) Sand roughness cemented to the surface

3. The mean-velocity distribution appears to afford a simple means of identifying a fully developed turbulent boundary layer.

4. The logarithmic laws of velocity distribution are not in good agreement with the measured distributions in the turbulent boundary layer with zero pressure gradient and are applicable only in a small region near the wall. The velocity profiles in the boundary layer are independent of Reynolds number on a velocity-defect basis, indicating a

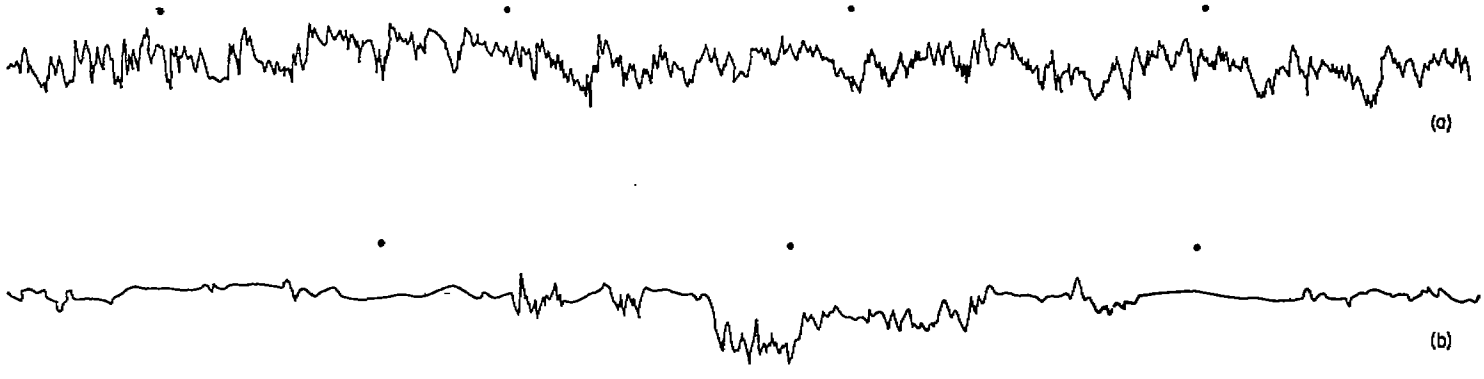

(a) $y/\delta=0.03$.
(b) $y/\delta=0.75$.

FIGURE 29.—Oscillograms of u-fluctuations in turbulent boundary layer. $x=10.5$ feet; $U_1=55$ feet per second; $\delta=3.1$ inches. Time interval between dots, 1/40 second. Boundary layer thickened by No. 16 sandpaper over first 2 feet of surface.

universal relationship of the form

$$\frac{U_1-U}{U_\tau}=f(y/\delta)$$

where U is the mean velocity in the boundary layer, U_1 is the mean velocity in the free stream just outside the boundary layer, U_τ is the square root of the ratio of the shearing stress at the surface to the density, y is the distance normal to the surface measured from the surface of a flat plate, and δ is the boundary-layer thickness.

5. The longitudinal scale of turbulence L_x in a fully developed layer is proportional to the boundary-layer thickness δ, with a value of L_x/δ of approximately 0.4, and except near the wall is constant across the layer.

6. There is a systematic variation in the one-dimensional energy spectrum across the boundary layer up to $y/\delta=0.6$, and in the outer region of the boundary layer, that is, $y/\delta>0.6$, the existing theories for the spectrum in isotropic turbulence can be applied.

7. There is an intermittent character to the flow in the turbulent boundary layer similar to that found for wakes and jets.

NATIONAL BUREAU OF STANDARDS,
WASHINGTON, D. C., *September 15, 1950.*

REFERENCES

1. Kolmogoroff, A. N.: The Local Structure of Turbulence in Incompressible Viscous Fluid for Very Large Reynolds' Numbers. Comp. rend., Acad. Sci. URSS, vol. 30, no. 4, Feb. 10, 1941, pp. 301–305.
2. Kolmogoroff, A. N.: Dissipation of Energy in the Locally Isotropic Turbulence. Comp. rend., Acad. Sci. URSS, vol. 32, no. 1, July 10, 1941, pp. 16–18.
3. Townsend, A. A.: Local Isotropy in the Turbulent Wake of a Cylinder. Australian Jour. Sci. Res., ser. A, vol. 1, no. 2, June 1948, pp. 161–174.
4. Corrsin, Stanley, and Uberoi, Mahinder S.: Spectra and Diffusion in a Round Turbulent Jet. NACA Rep. 1040, 1951. (Supersedes NACA TN 2124.)
5. Laufer, John: Investigation of Turbulent Flow in a Two-Dimensional Channel. NACA Rep. 1053, 1951. (Supersedes NACA TN 2123.)
6. Schubauer, G. B., and Klebanoff, P. S.: Investigation of Separation of the Turbulent Boundary Layer. NACA Rep. 1030, 1951. (Supersedes NACA TN 2133.)
7. Dryden, Hugh L., and Schubauer, G. B.: The Use of Damping Screens for the Reduction of Wind-Tunnel Turbulence. Jour. Aero. Sci., vol. 14, no. 4, April 1947, pp. 221–228.
8. Schubauer, G. B., and Klebanoff, P. S.: Theory and Application of Hot-Wire Instruments in the Investigation of Turbulent Boundary Layers. NACA WR W-86, 1946. (Formerly NACA ACR 5K27.)
9. Kovásznay, L.: Calibration and Measurement in Turbulence Research by the Hot-Wire Method. NACA TM 1130, 1947.
10. Liepmann, Hans W., and Fila, Gertrude H.: Investigations of Effects of Surface Temperature and Single Roughness Elements on Boundary-Layer Transition. NACA Rep. 890, 1947. (Supersedes NACA TN 1196.)
11. Hama, Ryosuke: Turbulent Boundary Layer along a Flat Plate. I and II. Rep. Inst Sci. and Technol., Tokyo Univ., vol. 1, no. 1, Jan. 1947, pp. 13–16; nos. 3–4, March–April 1947, pp. 49–50.
12. Schultz-Grunow, F.: New Frictional Resistance Law for Smooth Plates. NACA TM 986, 1941.
13. Fluid Motion Panel of the Aeronautical Research Committee and Others (S. Goldstein, ed.): Modern Developments in Fluid Dynamics. Vol. II. The Clarendon Press (Oxford), 1938, pp. 331–359.
14. Freeman, Hugh B.: Force Measurements on a 1/40-Scale Model of the U. S. Airship "Akron." NACA Rep. 432, 1932.
15. Nikuradse, J.: Gesetzmassigkeiten der turbulenten Stromung in glatten Rohren. Forschungsheft 356, VDI-Verlag G. m. b. H. (Berlin), 1932.
16. Nikuradse, Johann: Untersuchungen über die Strömungen des Wassers in konvergenten und divergenten Kanälen. Forsch.-Arb. Geb. Ing.-Wes., Heft 289, 1929.
17. Dönch, Fritz: Divergente und konvergente turbulente Strömungen mit kleinen Öffnungswinkeln. Forsch.-Arb. Geb. Ing.-Wes., Heft 282, 1926.
18. Millikan, Clark B.: A Critical Discussion of Turbulent Flows in Channels and Circular Tubes. Proc. Fifth Int. Cong. Appl. Mech. (Sept. 1938, Cambridge, Mass.), John Wiley & Sons, Inc., 1939, pp. 386-392.
19. Heisenberg, W.: Zur statistischen Theorie der Turbulenz. Zeitschr. Phys., Bd. 124, Heft 7/12, 1948, pp. 628–657.
20. Taylor, G. I.: Statistical Theory of Turbulence. Part I. Proc. Roy. Soc. (London), ser. A, vol. 151, no. 873, Sept. 2, 1935, pp. 423–444.
21. Townsend, A. A.: Momentum and Energy Diffusion in the Turbulent Wake of a Cylinder. Proc. Roy. Soc. (London), ser. A, vol. 197, no. 1048, May 11, 1949, pp. 124–140.
22. Corrsin, Stanley: Investigation of Flow in an Axially Symmetrical Heated Jet of Air. NACA WR W-94, 1943. (Formerly NACA ACR 3L23.)

U. S. GOVERNMENT PRINTING OFFICE: 1954